SUPPORTING STUDIES IN CLOUD IMAGE PROCESSING FOR PLANETARY FLYBYS OF THE 1970'S

Semi-Annual Progress Report
for the period
1 July 1975 through 31 December 1975

NASA Grant NCR 50-002-189

V. E. Suomi, Principal Investigator
R. J. Krauss, Program Manager

Space Science and Engineering Center
University of Wisconsin-Madison
1225 West Dayton Street
Madison, Wisconsin 53706

31 December 1975

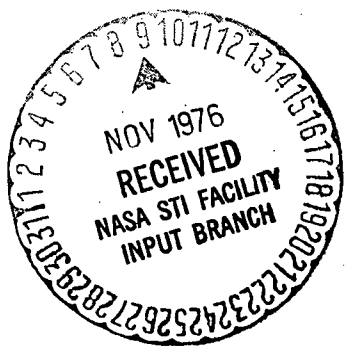

PROGRAM STATUS REPORT

Progress has continued swiftly through the summer months. Three more Venus data sets have been navigated and measurements begun, extending the time base out to nearly two days of the 8 day mission. The motion field is evidencing more complexity and structure than we had thought, so the JAS paper we had intended to write on Venus cloud motions has been indefinitely postponed until we can make a definitive statement on the subject. We will continue to communicate with the science community in a less formal manner, however, through personal communication and presented papers.

Sanjay Limaye, one of Professor Suomi's meteorology Ph.D. candidates will be fully supported by this grant during the coming year, and will do his thesis on the subject of Venus. One of his first research papers, dealing with normalized images of Venus is attached as Appendix A. It will be presented at the American Astronomical Society meeting in Austin, Texas, at the end of March, and then will be submitted to the Journal of Atmospheric Sciences for publication.

Limaye has extended the Mariner 10 navigation model developed by Phillips to remove the effect of lighting conditions (sun zenith angle) and viewing conditions (spacecraft zenith angle) in the Venus images. A photometric function based on Chandrasekhar's H-functions can be applied to the image data which will change the brightness level of every cloud element to that which it would have if it were on a plane, illuminated by plane parallel light, and then viewed from infinitely far away. This permits the Venus clouds in any Mariner 10 image to be corrected so they have a brightness directly proportional to the true albedo, which is closely dependent on optical depth, or thickness. The clouds can then be analyzed to study growth rates and changes, or one can measure divergence or eddy transport independent of the effects of geometry or phase angle. The technique

will be used primarily to infer vertical motions in the equatorial regions of Venus and to investigate cloud thickness or any other properties which may be masked or altered by lighting conditions and geometry. A relation may exist between absolute cloud brightness and altitude, for example, which could be used to stratify the cloud motion fields in the vertical.

Plans to extend the Venus navigation scheme by means of a "leap-frog" approach have received a setback, as Dennis Phillips, our navigation expert, has taken a leave of absence to pursue his own research in applied mathematics. He will not be returning to SSEC to continue work on Venus until next summer. Appendix B is a report on the currently operational navigation scheme, written by Phillips and Sanjay Limaye. It gives mathematical details of the image alignment technique which forms the foundation of the Venus cloud motion determinations. The transforms used to convert from Mariner 10 image coordinates to cloud velocities are described. The technique is based on finding a simple least squares solution to the bright limb of the planet, thereby defining both the planet center and the scale of the latitude-longitude grid. The sun-planet-spacecraft geometry then defines image tilt, and permits definition of the orientation of the grid on the planet. This first paper on the navigation process serves as an introduction to a complex but highly necessary part of measuring cloud motions.

FUTURE PLANS

With the navigation project delayed until next summer, we have postponed investigation into small scale processes on Venus. Detailed analysis of the high resolution images will have to wait until we get all the "tools" assembled.

In the meantime, emphasis will be placed on getting the majority of far encounter images of Venus (days 39-43) navigated and measured. The three new data sets now being analyzed ought to be completed by late January or February and we plan to report on those results at the March DPS meeting as well.

Work is continuing in three other areas. We are attempting to gather enough 16mm film footage of our Venus data to show at the DPS meeting; we are working on developing a shear model of the spiral streaks on Venus, first reported by Murray, et.al. after the Mariner 10 Venus encounter; and Limaye will be extending some of his previous vertical lapse rate calculations by use of a real gas equation. The last two items should produce publishable papers.

Our Venus funding through JPL ended in October, so all further work at SSEC in Mariner image analysis will be funded solely by this grant.

APPENDIX A

P R E P R I N T
D R A F T

A NORMALIZED VIEW OF VENUS*

Sanjay Limaye and Verner Suomi

(To be Submitted to Journal of Atmos. Sci.)

*To be presented at the Division of Planetary Science Meeting of the American Astronomical Society, Austin, Texas, March 31-April 4, 1976

10 September 1975

Space Science and Engineering Center
University of Wisconsin, Madison 53706

ABSTRACT

It is now known that Venus has a fairly thick and massive atmosphere, the 10 mb level occurring at a height of about 80 km above the surface. Mariner 10 television observations agree with an isotropic scattering model with single scattering albedo of about 0.92 in the ultra-violet region of the spectrum (Hapke, 1975). Based on this knowledge, a few Mariner 10 images have been "normalized" to a standard scattering geometry using the exact solution by Chandrasekhar (1950) involving his H-functions.

The most striking feature of the normalized images is the bright polar ring or cap beyond about 50° latitude circle and a sharper brightness frequency distribution. The brightness variation along a meridian shows substantial axial symmetry on a large scale and small scale brightness variations over the planet are no more than about 10%. Such a normalized brightness profile along a meridian is suggestive of low optical depth above cloud tops in low latitudes and larger in polar latitudes, if the enhanced polar brightness is assumed to be due to increased scattering above the cloud tops.

The variation of mean brightness and of the ratio of mean square deviation of brightness to average brightness is comparable to the performance limits of the vidicon camera for the image sequence lasting about a day so that the variation in distribution of dark and bright features over the planet and the UV albedo of the planet over about a day is small.

1. Introduction

This paper deals with "normalization," of several Mariner 10 UV images of Venus based on the assumption of diffuse reflection by the cloudy atmosphere such that every point on the planet is viewed in the image with the same scattering geometry. This facilitates a comparison of the absolute brightness of the UV features in various regions of the sunlit planet. The terrestrial experience is that in a normalized image the general rule of thumb that brighter clouds are optically thicker can be quantified (Martin et al. 1975). The question of the ultraviolet contrasts in the atmosphere of Venus is still unsettled and it is not possible to postulate a general yardstick between the brightness of UV features and their optical and/or geometric thickness. Nevertheless, the sun and viewing angle normalized images show up some interesting characteristics.

It was pointed out by Huggins (1867) that optically thick planetary atmospheres would behave roughly like Lambertian reflectors. This was confirmed by observations of Mars from Mariner 9 (Leovy et al. 1972) even though the Martian atmosphere is thin compared to that of Venus.

Horak (1950) reported that the visual and photographic curves for Venus can be represented by known laws of diffuse reflection for phase angles less than 130° with isotropic scattering and a single scattering albedo $\tilde{\omega}_o = 0.950$. It is interesting to note that the limb darkening in yellow light can also be represented fairly well by isotropic scattering again with $\tilde{\omega}_o = 0.950$ and that the polarization of the atmosphere of Venus is not due to Rayleigh scattering (Horak, 1950).

Hapke (1975) has found similar results from observations of the UV images from Mariner 10. In particular, a single scattering albedo

$\tilde{\omega}_o$ between 0.91 and 0.93 with isotropic scattering agrees very well with the observations, better than results from Mie scattering or Rayleigh scattering.

Using a mean single scattering albedo in the law of diffuse reflection, it is possible to normalize a Mariner 10 Venus image to a standard sun-planet-camera geometry for every point on the planet so that the brightness variations in a normalized image represent actual physical characteristics of the features alone and are not due to different solar and spacecraft (camera) zenith angles.

2. Image normalization

a. Fig. 1 shows, the intensity along a particular image scan line passing through both the subsolar and the subspacecraft point in the normalized version of a UV image (FDS #64897). The solid line represents the mean H-function solution for $\tilde{\omega}_o = 0.92$, based on Hapke's (1975) results that isotropic scattering models with $\tilde{\omega}_o$ between 0.91 and 0.93 match with observed intensities. The departures from the mean photometric curve are the Venusian light and dark features. The images analyzed were corrected for geometric distortion as well as for photometric deviations at the Image Processing Laboratory (IPL) of Jet Propulsion Labs.

Mariner 10 images of Venus show a large number of atmospheric features in the ultraviolet, and the observed contrast is generally fairly small. In particular, one sees a few recurrent bowlike features which seem to move at approximately the same speed as other features without drastically changing their shape or size.

In other regions of the planet 'cloud-clusters' or large bright patchy features move from the morning terminator side toward the subsolar

region rapidly changing their shape and brightness. As seen in the "raw" sequence in Fig. 3, (left), there are certain features which show a marked change in their overall brightness as they move across the planet. Since the solar and camera zenith angles vary substantially for a certain feature as it moves across the planet disc, it is not immediately clear whether the observed changes in the overall brightness of a feature are real and whether they are simply due to a change in illumination and viewing angles. The normalization of a sequence of Mariner 10 Venus image would ensure that any changes in the brightness of a feature as it moved across the planet would be due to actual physical changes in the feature and not be due to changing scattering geometry. Thus, standardizing every point on the planet to the same sun-camera geometry enables us to gain information about the properties of the features themselves.

b. Normalization procedure

Chandrasekhar (1950) has obtained the exact solution for the case of diffuse reflection from a plane parallel atmosphere as follows:

$$I(o,\mu) = \frac{\tilde{\omega}_o F}{4\pi} \left(\frac{\mu_o}{\mu_o + \mu}\right) H(\mu)\ H(\mu_o) \qquad (1)$$

Where I is the emergent intensity, πF is the flux incident on the planet, $\tilde{\omega}_o = \cos \zeta$ is the cosine of the solar zenith angle, and $\mu = \cos \eta$ is the zenith angle of the camera. The isotropic scattering phase function $P(\cos \Theta) = \tilde{\omega}_o$ has been used, wherein $\tilde{\omega}_o$ is the single scattering albedo. $H(\mu)$ and $H(\mu_o)$ are Chandrasekhar H-functions, and tabulated values are available (Chandrasekhar, 1950). Fig. 2 shows the values of $H(\mu)$ for various values of the single scattering albedo $\tilde{\omega}_o$.

For normalizing an image, we introduce an arbitrary scaling constant $X(\lambda,\phi)$ to describe the light and dark features seen on the planet in (1):

$$I_{OBS} = \frac{\tilde{\omega}_o F}{4\pi} \left[\left(\frac{\mu_o}{\mu_o + \mu}\right) H(\mu)\, H(\mu_o)\right] X(\lambda,\phi).$$

So that $\frac{F}{4\pi} X(\lambda,\phi)$ is the normalized brightness for the point (λ,ϕ) on the planet, given by:

$$I^* = \frac{F}{4\pi} X(\lambda,\phi) = I_{OBS} \frac{(\mu_o + \mu)}{\tilde{\omega}_o \mu_o\, H(\mu)\, H(\mu_o)}.$$

One then needs to know the single scattering albedo $\tilde{\omega}_o$, and the two zenith angles ζ and η for the sun and spacecraft in order to obtain the normalized brightness for every point.

To be able to compute $\mu_o = \cos\zeta$ and $\mu = \cos\eta$ the image has to be navigated first (i.e. to obtain a transform between the image plane coordinates of a point $P(\ell,e)$ where ℓ is the scan line number and e the sample element number in that scan line) to the absolute position $P(\lambda,\phi)$ in latitude and longitude on the planet:

$$T(\ell,e,\lambda,\phi)\; P(\ell,e) = P(\lambda,\phi)\ .$$

The coordinate transformation function $T(\ell,e,\lambda,\phi)$ can be obtained from a knowledge of the spacecraft orbit parameters and the location of the sub-solar point and the sub-spacecraft point with the crucial constraint that the sub-solar point and the sub-spacecraft point lie on the same image scan line. A more detailed description of image navigation is given by Phillips and Limaye (1975).

The H-functions for the zenith angles are then computed by a four point Lagrangian interpolation scheme from the tabulated values given by Chandrasekhar (1950).

3. Discussion

The unnormalized and normalized versions of the 12-image sequence on Julian day 40, 1974 are shown in Fig. 3 in the left and right columns

respectively. The unnormalized versions were decalibrated using the program FICOR at the Image Processing Laboratory of the Jet Propulsion Laboratory, so that the digital brightness numbers are related linearly to the actual intensity at least at brightness numbers greater than about 10 on a 0 to 255 scale. During the normalization of the images it was ensured that the dynamic range of all the images was between 0 and 255 and that there were no saturation. Thus a comparison of the brightness of a feature in successive frames is possible and is limited only by the absolute accuracy limit of the vidicon. The brightness changes observed in the normalized sequence are thus indicative of actual changes in the scattering characteristics of the features in terms of their shape, size and scatterers as long as they are greater than the accuracy limits of the vidicon.

Within a single frame the relative photometric accuracy of the vidicons is believed to be about $\pm$3% and the absolute accuracy is believed to be about $\pm$10% (Hapke et al. 1975).

Fig. 4 shows a comparison of brightness frequency histograms for the original and normalized versions of a typical Mariner 10 UV image. The normalized version shows a bi-modal distribution, the lower peak corresponding to higher brightness values is due to brighter polar region and the median polar region brightness is about 50% higher than the equatorial value.

a. Mean brightness and RMS deviation

It is known that the contrast in the UV images of Venus is scale dependent (Hapke, 1975). On a global scale when the phase angle is small, the contrast of the whole disc depends on the distribution of bright and dark features which are reported to move across the disc at speeds

between 80 and 130 m/s (Suomi, 1975). Any large spatial dependence of bright and dark features in the upper atmosphere should thus show up in a time series of pictures monitored for contrast. Fig. 5 shows variation of contrast c, the ratio of RMS brightness number deviation σ and the mean brightness number $\overline{B}$ for eleven UV images on Julian Day 40. The solar zenith angle at the sub-spacecraft point decreased from 29.12° in the beginning of the sequence to 28.16° at the end of the sequence. Two of the images were partial images.

The mean brightness of the visible disc in both the raw and the normalized versions show a slow monotonic decrease, ignoring the small variations due presumably to the performance characteristics of the vidicon. *This monotonic decrease in mean brightness is accompanied by* a slow increase in contrast c ($=\sigma/\overline{B}$) (Fig. 6), and the two are indicative of a large UV dark feature moving into the visible hemisphere from the nightside over the duration of the sequence ($\sim$ 18 hours).

The variation in the contrast in raw images is not more than 1% over the sequence and thus the number of light and dark features over the visible planet and the UV albedo over this 18 hour period can be considered to be constant.

The reduced overall contrast in the normalized images occurs due to the removal of the gradual changes in the scattering angle over the planet as evidenced by the constant 'mean' brightness variation in the normalized version (Fig. 1b). The normalization procedure reduces the contrast for values of normalization factor less than 1, i.e. for low sun and spacecraft zenith angles and enhances it for larger sun and spacecraft zenith angles when the normalization factor is greater than unity.

b. The bright polar region

The meridional variation of uncorrected and normalized brightness along meridians through the subsolar and the subspacecraft points are shown in Figs. 7a and 7b respectively. The two normalized profiles show virtually identical large-scale brightness variations, and the small scale variations, which are the signatures of the UV features, are less than about 10%, thus indicating the small longitudinal dependence of brightness. The normalized profiles show a much lower brightness in the equatorial region than in the polar regions.

The edge of the southern bright polar cloud or ring is around about 52° latitude. An indication of a similar bright polar cloud in the northern hemisphere at about the same latitude can be seen. Unfortunately, the flyby trajectory of Mariner 10 was unsuitable for imaging the north polar region. Dolfuss (1974) has examined earth-based photographs of Venus over a long period and reports a variability in the appearance of the polar clouds. They seem to appear and disappear periodically, and all four cases - (i) both the polar cloud (ii) northern polar cloud only (iii) southern polar cloud only and (iv) no polar cloud, have been observed. From the observation of the bright patch in the northern hemisphere, it seems that Venus had two polar clouds at the time of the Mariner 10 encounter.

The high contrast between the polar clouds and the subpolar region is indicative of different atmospheric scattering conditions in those regions. The increase in the brightness of the polar clouds can be seen in Fig. 7 which is a plot of brightness along a meridian. At present, there is no evidence regarding the constituents in the bright polar clouds responsible for scattering ultra-violet light, and this enhanced brightness is a puzzle.

There is a possiblity that the thermal structure may reflect the existence of the polar clouds. The infrared radiometer on-board the Mariner 10 made one swath across the planet in the northern hemisphere, and in the 45μ band the departure from the linear limb darkening law is maximum at the longitude of closest approach to the northern polar ring (Chase et al. 1974). The deviation from the linear limb darkening law decreases sharply as the radiometer field-of-view moves away from the suspected position of the edge of polar clouds. It is quite possible that the associated lower brightness temperature on either side of closest approach to the polar cloud edge is related to the existence of the norther polar ring. The southern polar ring counterpart seems to be a continual feature of the UV images during the duration of Mariner 10 coverage.

Calculations by Ingersoll and Orton (1974) of the sun-associated component of the brightness temperature indicate that at least on the night side at about 50° latitude the temperature is approximately 7 K lower than at the equator. This might be the case on the day-side also. It is likely that this brightness temperature corresponds to the "cloud top" temperatures and that such cloud tops are seen as UV features in the UV images. As the above authors point out, it is difficult to resolve the observed brightness temperature variations into horizontal and vertical components from available data. It is known that at least in the lower latitudes, the atmosphere is very stable with a subadiabatic lapse rate of 4-5° K km^{-1} (Howard et al. 1974). Assuming similar lapse conditions at higher latitudes the lower cloud tops in polar regions could have a lower brightness temperature if the actual temperature decreases on a level surface towards the poles sufficiently.

It is possible then that this polar regions of enhanced brightness has

lower "cloud tops" than its equatorial counterpart with a somewhat lower brightness temperature. If this is the case then there is likely to be more Venus air mass (mostly carbon dioxide) gas above the polar clouds than over the rest of the planet and spectroscopic observations of carbon dioxide line strengths with sufficient spatial resolution should be able to detect it.

From ground based spectroscopic measurements Young et al. (1973) finds that while the correlation between the carbon dioxide abundance over the cloud tops and dark and light UV markings is not obvious, there is an indication that there is more carbon dioxide above the brighter areas. If this is true this lends support to the hypothesis that the cloud tops in the polar regions are lower than in the equatorial regions and the brightness temperature in those regions is lower due to a north-south horizontal temperature gradient--large enough to offset the higher cloud top temperatures.

If the polar clouds have tops lower in altitude, then the cloud-top pressure regions are thus likely to be higher and hence the equivalent bandwidth of carbon dioxide lines must be larger near the south pole than at the equator. Moroz (1971) reports this exact finding: the 1.6μ band observations indicate that the pressure there is considerably higher than at a similar level for the equatorial regions and argues that the polar cloud tops may be 4-7 km lower than in the equatorial region. There is other evidence available.

More recent observations of Barker and Perry (1975) of the carbon dioxide line strengths indicate that the south polar carbon dioxide abundance (presumably above the 'visible' cloud tops) is about 8% greater than that over the equatorial region. Some of their reported observations taken through the 100 inch telescope at McDonald observatory coincided with the Venus encounter of Mariner 10 (Julian days 38-40, 1974). It is quite likely that this

difference in relative abundance of carbon dioxide is actually higher than the observed value since the spatial resolution of ground based observations even near inferior conjunction is quite small, and thus observations of Barker and Perry (1975) are mean values over a large area.

As mentioned earlier the lower temperature in polar regions may cause phase changes in the cloud constituents and hence the light scattered by the cloud in the UV. Thus while increased scattering in the UV by higher amount of carbon dioxide gas above the cloud-top is a likely cause for enhanced polar brightness, it need not be the only one.

Lastly, it is possible to place an upper limit on the possible altitude difference between the equatorial and polar cloud tops if one assumes a certain meridional temperature variation. For example, it can be shown that for a cosine decrease of temperature with latitude, the maximum equator to pole temperature contrast that can be maintained through global radiative balance is about 70°K. For an average lapse rate of about 5 K km^{-1} above 65 km altitude everywhere, and noting that the surface polar temperature seems to be at least as high, if not higher, than the equatorial temperature from microwave measurements (Sinclair et al., 1972), the polar cloud tops can therefore only be a maximum of about 14 km lower than the equatorial cloud tops. However, the actual temperature difference is probably much smaller as well as the cloud top altitude difference.

c. Transition zone

At this point it is interesting to note that the zonal component of the motion of UV features as revealed by Mariner 10 images shows a maximum somewhere between 45° and 50° latitude in the southern hemisphere (Suomi, 1974). Poleward of that the zonal component is smaller and must vanish at the pole. The meridional shear of such a profile is quite large beyond the latitude of

maximum zonal wind and according to the Rayleigh criterion this is the favored zone for onset of barotropic instability. The exact latitude for the instability is given by the necessary and sufficient condition that the absolute vorticity vanish. The equatorial edge of the polar clouds in the normalized image sequence is around about 52° latitude circle i.e. close to the latitude of maximum zonal component of motion of UV features. It is tempting to suggest that the polar clouds are related to a dynamic instability--perhaps barotropic.

In this transition zone around about 50° latitude which contains the latitude of maximum zonal motion of UV features and on the poleward side of which the cloud tops appear to be at a lower altitude than on the equatorial side, the situation is similar to the terrestrial atmosphere in the vicinity of a front. Admittedly a front for example a polar front on earth is a baroclinic zone, however on Venus the maximum temperature differences are quite small so that in effect a small temperature contrast of a few degrees may have effects similar to a state of baroclinicity. In the case of Venus there is evidence to believe that:

(i) a zonal wind maximum exists,

(ii) the cloud tops at different altitudes on either side of the zone of maximum zonal wind,

(iii) large horizontal shear in atmospheric flow in the vicinity of the maximum wind region, and

(iv) likely high vertical wind shear in the vicinity of periphery of polar clouds.

Thus this transition zone in the upper atmosphere of Venus at the level of cloud-free tops has most of the properties of a frontal zone. It is important therefore to determine the meridional temperature gradient and the wind shear

across this zone from future observations such as those from the Pioneer Venus Multiprobe Mission.

The upper atmospheric dynamics and the large scale polar-equatorial brightness difference appear to be very closely related. The cloud tops in latitudes higher than about 50° are hypothesized to occur at lower altitudes to explain their enhanced brightness by increased scattering in the atmosphere overlying them. In order to be consistent with only a weak meridional gradient of sun-associated brightness temperature, there has to be a compensating isobaric or isohypsic meridional temperature gradient, assuming nonisothermal, subadiabatic lapse rates in that part of the atmosphere. Needless to say, under steady state conditions the meridional heat transport must be such as to be able to maintain the required meridional thermal contrasts.

4. Summary and recommendations

A sequence of Mariner 10 Venus images have been normalized according to an exact solution obtained by Chandrasekhar (1950) for the problem of diffuse reflection from a semi-infinite plane parallel atmosphere. The isotropic scattering phase function with single scattering albedo of 0.92 based on Hapke's results (1975) was used for normalization. A sequence of images normalized in this fashion helps identify physical changes in the UV features seen in the image sequence by isolating them from effects of varying scattering geometry.

The south polar cap stands out as the brightest part of the image with little contrast. The subsolar region is relatively dark. The high brightness of the polar cap is suggestive of significantly different atmospheric conditions.

The mean brightness of the planet over the sequence of images studied varies only by about 7%. This should perhaps be interpreted to be the performance limit ($\sim \pm 4\%$) of the vidicon rather than an appreciable change in UV albedo of the planet due to uncertainties in vidicon calibration. The contrast, defined as the ratio of RMS deviation from the mean brightness and the mean brightness increases gradually over the sequence and is associated with the movement of a large UV dark feature into the visible hemisphere from the nightside.

It is strongly recommended that at least one of the atmospheric probes from the next Pioneer mission to Venus be launched so as to probe the atmosphere in the polar cap region. Temperature profiles obtained through radio occultations from the Venus orbiter would give valuable information about the 3-D thermal contrasts in the atmosphere.

Maps of carbon dioxide abundances with the high enough spatial resolution might prove to be valuable in understanding the UV contrasts on Venus, in particular the pole-equator differences. Thermal infrared maps will also be useful in finding an answer to this riddle.

ACKNOWLEDGEMENTS

The authors express thanks to the people at the Image Processing Lab at JPL, Pasadena, Calif. for providing photometrically and geometrically corrected pictures. We are thankful to Mr. Fred Mosher and to Mr. Robert Krauss for the discussions and to Drs. Bruce Hapke and Michael Belton for their critical comments. Lastly, we appreciate the programming help of Messrs. Eric Smith, Dennis Phillips, and Ralph DeDecker.

This research was supported by NASA Contract #NGR-50-002-189.

LIST OF FIGURES

large scale brightness variations. (Thick line through subsolar point, thin line through subspacecraft point.)

Figure 7b Same as Figure 7a except for the normalized version. The polar regions enhanced brightness and a rather sharp transition zone.

REFERENCES

Barker, E. D. and M. A. Perry, 1975: Semiperiodic Variations in CO_2 Abundance on Venus, ICARUS, (25), 282-295.

Chandrasekhar, S., 1950: Radiative Transfer Theory. Clarendon Press, Oxford, 381 pp.

Chase, S. C., E. D. Miner, D. Mirrison, G. Munch, and G. Neugebauer, 1974: Preliminary Infrared Radiometry of Venus from Mariner 10, Science, (183), 1292-1293.

Dolfuss, A., 1974: Paper presented at the Conference on Atmosphere of Venus, Goddard Inst. of Space Studies, New York, 15-17 Oct.

Hapke, B., G. E. Danielson, K. Klaasen, and L. Wilson, 1975: Photometric Observations of Mercury from Mariner 10. J. Geophys. Res., (80), 2431-2443.

Hapke, B., 1975: Photometry of Venus from Mariner 10. To be published in Journ. Atmos. Sci.

Horak, H. G., 1950: Diffuse reflection by Planetary Atmospheres, Astrophys. Journ., (112), 445-463.

Howard, H. T., G. L. Tyler, G. Fjeldbo, A. J. Kliore, G. S. Levy, D. L. Brunn, R. Dickinson, R. E. Edelson, W. L. Martin, R. B. Postal, B. Seidel, T. T. Sesplauleis, D. L. Shirley, C. T. Stelzried, D. N. Sweetnam, Z. I. Zygielbaum, P. B. Esposito, J. D. Anderson, I. I. Shapiro, and R. D. Reasenberg, 1974: Venus: Mass, Gravity Field, Atmosphere, and Ionosphere as Measured by the Mariner 10 Dual Frequency Radio System. Science, (183), 1297-1306.

Huggins, W., 1867: On the Spectrum of Mars, With Some Remarks on the Colour of that Planet. Month. Notice Roy. Astron. Soc. (27), 178-181.

Ingersoll, A. P. and G. S. Orton, 1974: Lateral Inhomogeneities in the Venus Atmosphere: Analysis of Thermal Infrared Maps. ICARUS, (21), 121-128.

Leovy, C. B., G. A. Briggs, A. T. Young, B. A. Smith, J. B. Pollack, E. N. Shipley, and R. L. Wildey, 1972: The Martian Atmosphere: Mariner 9 Television Experiment Progress Report. ICARUS, (17), 373-393.

Martin D. W., J. Stout, and D. N. Sikdar, 1975: GATE Area Rainfall Estimation from Satellite Images. (See Appendix B of F. Mosher: Brightness Normalization of Satellite Images.) A report on NOAA Grant 04-5-158-47, Space Science and Engineering Center, Madison, University of Wisconsin, Madison.

Moroz, V. I., 1971: Polar Tropopause on Venus. Soviet Astronomy-AJ, (15), 448-453.

Phillips, D. and S. S. Limaye, 1975: Navigation of Mariner 10 Images of Venus. Space Science and Engineering Center, University of Wisconsin, Madison, Annual Report.

Sinclair, A. E. C., J. P. Basart, D. Buhl and W. A. Gale (1972): Precision Interferometric Observations of Venus at 11.1 cm Wavelength. Astrophys. J.,(175), 555-572.

Suomi, V. E., 1974: Mariner 10 Observations of Cloud Motions. Presented at the Conference on the Atmosphere of Venus, Goddard Institute of Space Studies, 15-17 Oct. 1974. [Also NASA-Report SP-382 (1975)]

Young, L. G., A. T. Young, J. W. Young, and J. T. Bergstralh, 1973: The Planet Venus: A New Periodic Spectrum Variable. Astrophys. J., (181), 15-18.

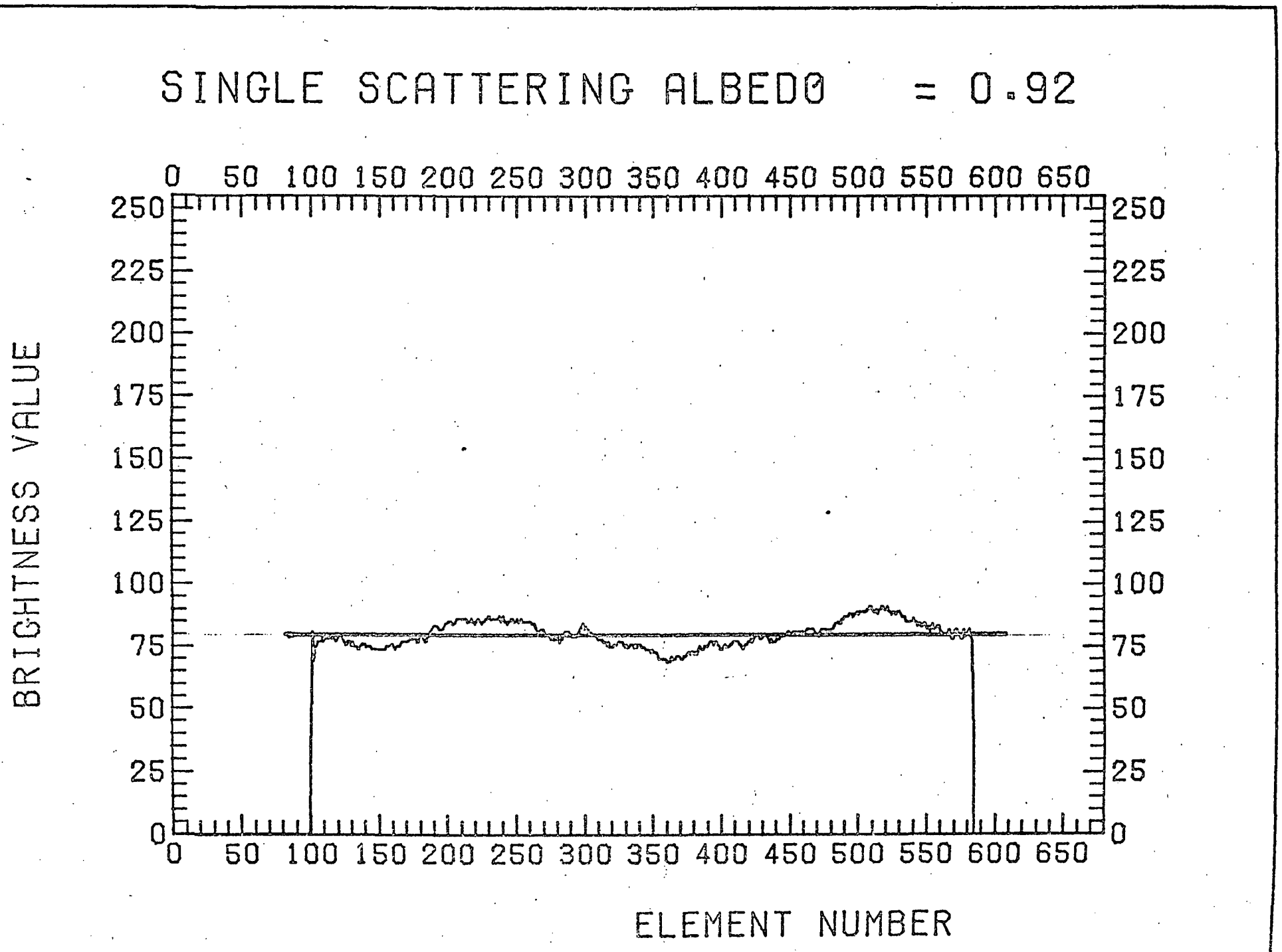
SINGLE SCATTERING ALBEDO = 0.92
BRIGHTNESS VALUE
ELEMENT NUMBER
0 50 100 150 200 250 300 350 400 450 500 550 600 650
250 225 200 175 150 125 100 75 50 25 0

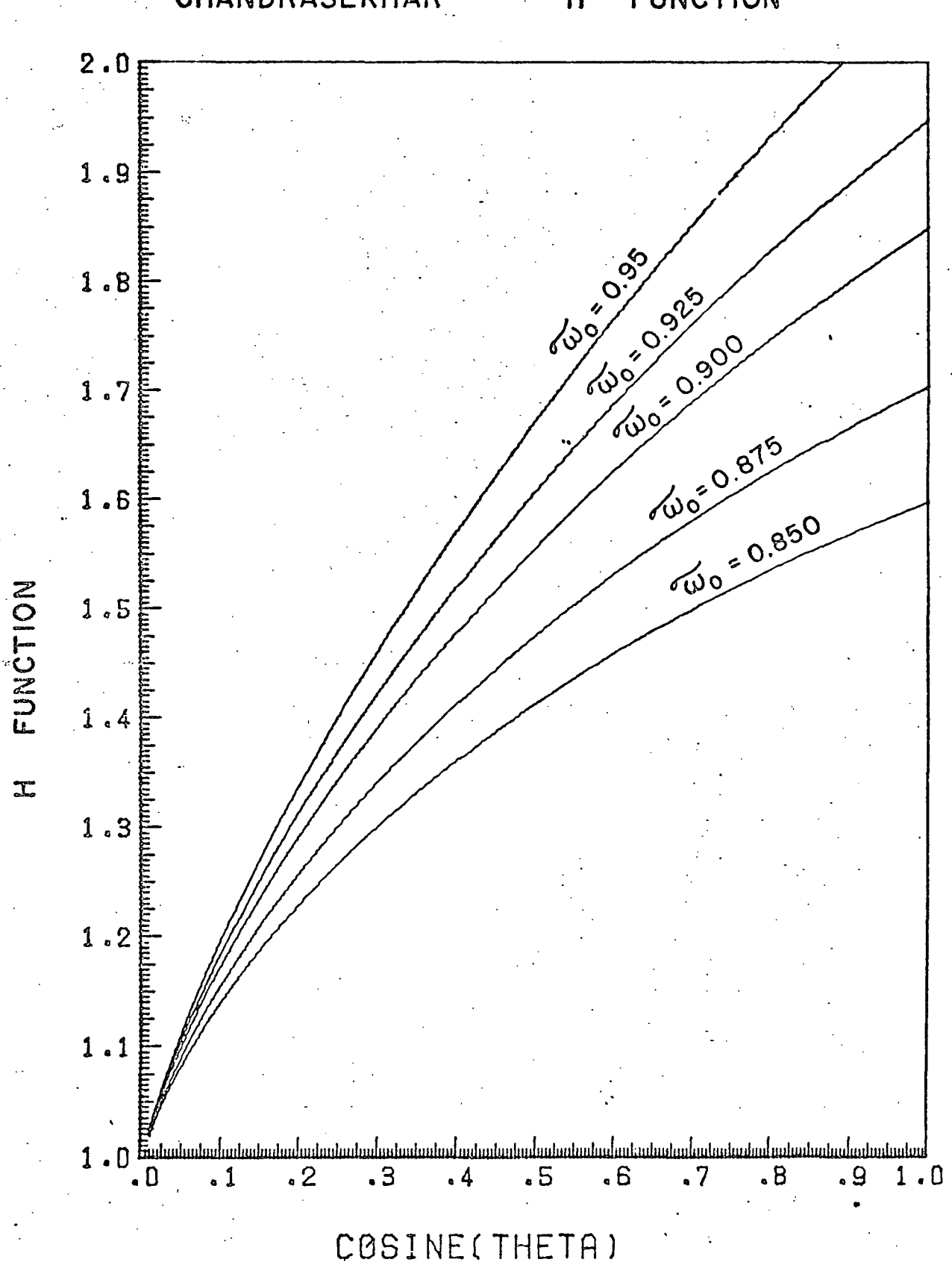
CHANDRASEKHAR H FUNCTION
H FUNCTION
2.0
1.9
1.8
1.7
1.6
1.5
1.4
1.3
1.2
1.1
1.0
.0
.1
.2
.3
.4
.5
.6
.7
.8
.9
1.0
COSINE(THETA)
ϖ0 = 0.95
ϖ0 = 0.925
ϖ0 = 0.900
ϖ0 = 0.875
ϖ0 = 0.850

UNCORRECTED VERSION

NORMALIZED VERSION

J. DAY 40, 1974

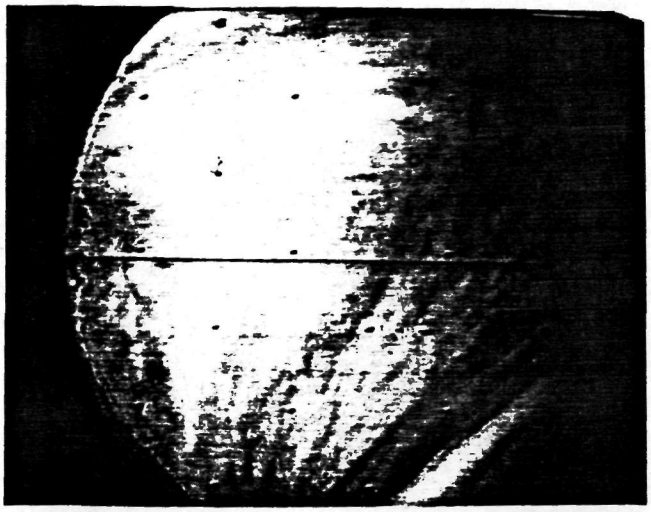

FDS # 64747 02 04 44 GMT

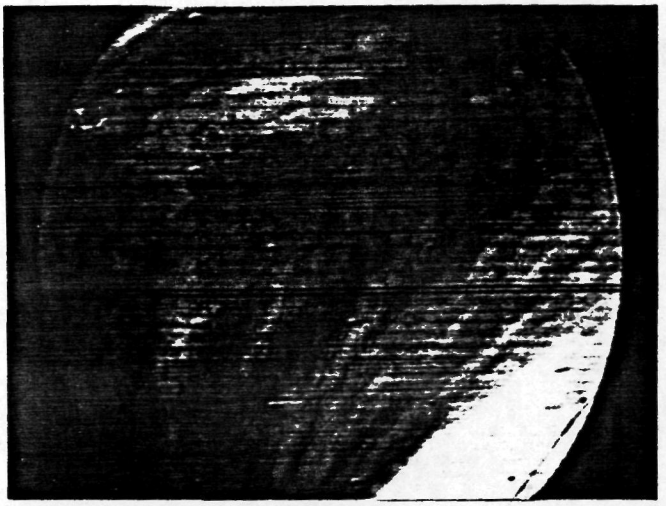

FDS # 64747 02 04 44 GMT

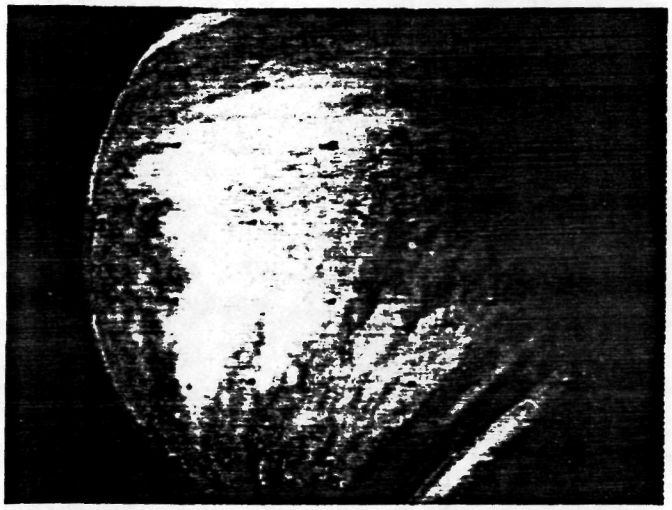

FDS # 64897 03 49 44 GMT

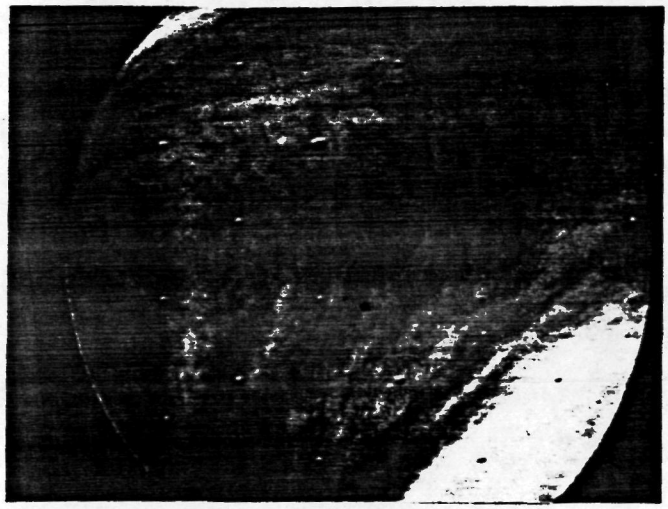

FDS # 64897 03 49 44 GMT

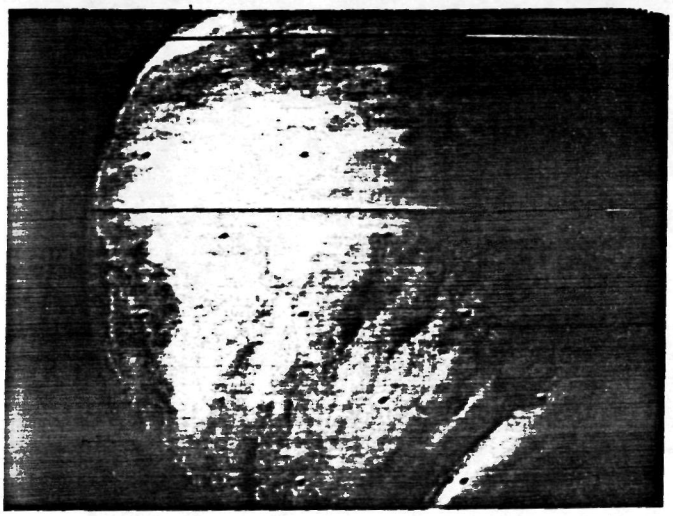

FDS # 65023 05 17 56 GMT

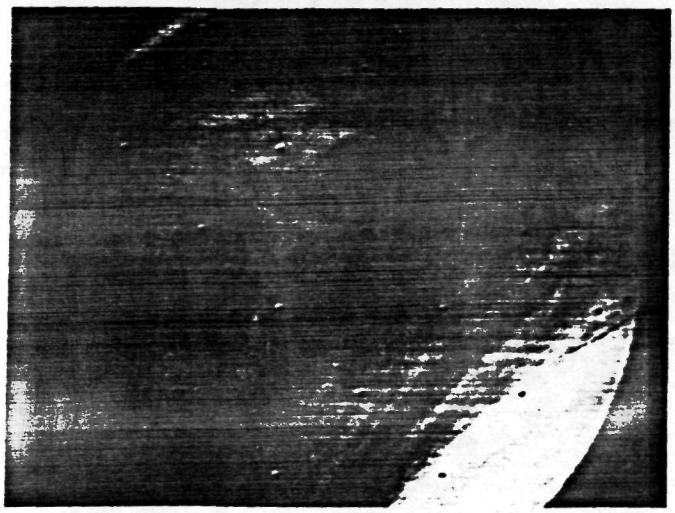

FDS # 65023 05 17 56 GMT

UNCORRECTED VERSION

NORMALIZED VERSION

J. DAY 40, 1974

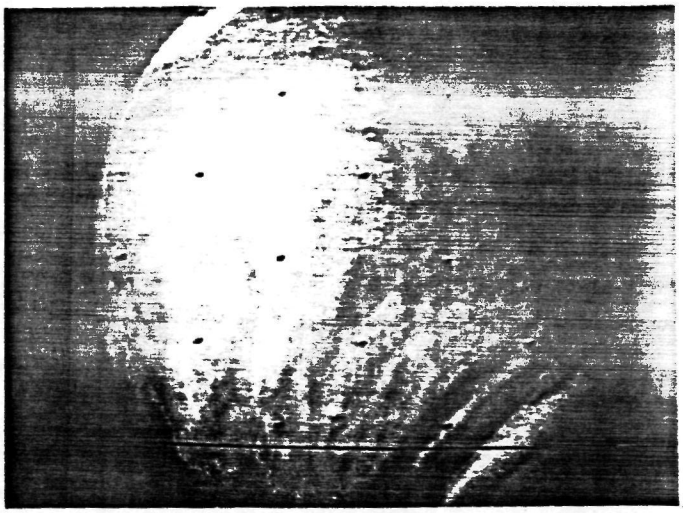

FDS # 65179 07 07 08 GMT

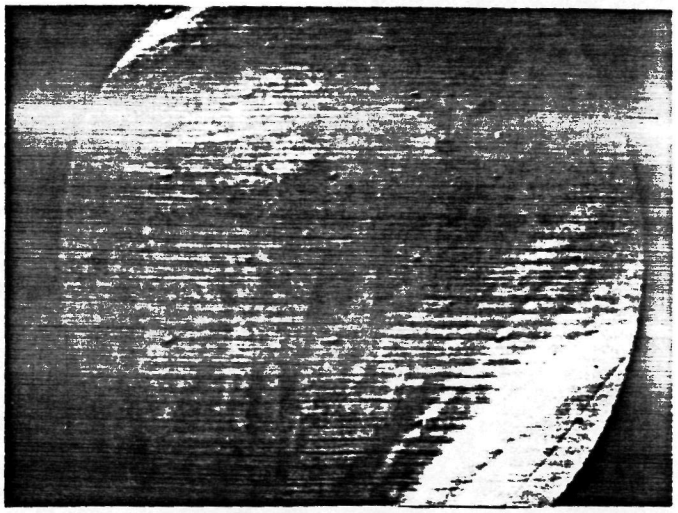

FDS # 65179 07 07 08 GMT

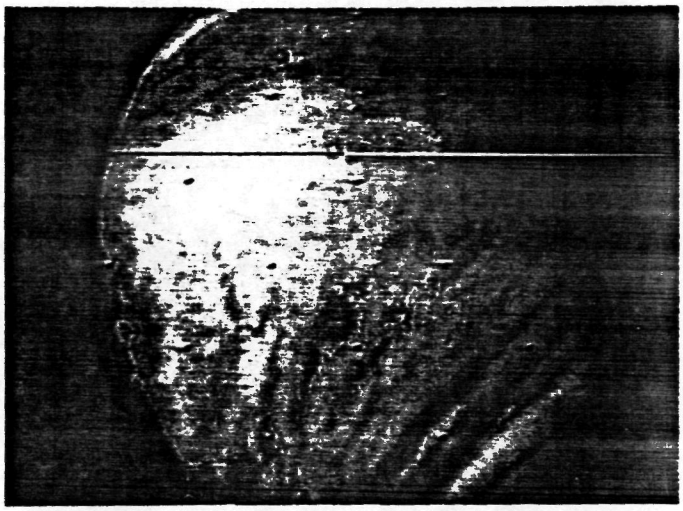

FDS # 65343 09 01 56 GMT

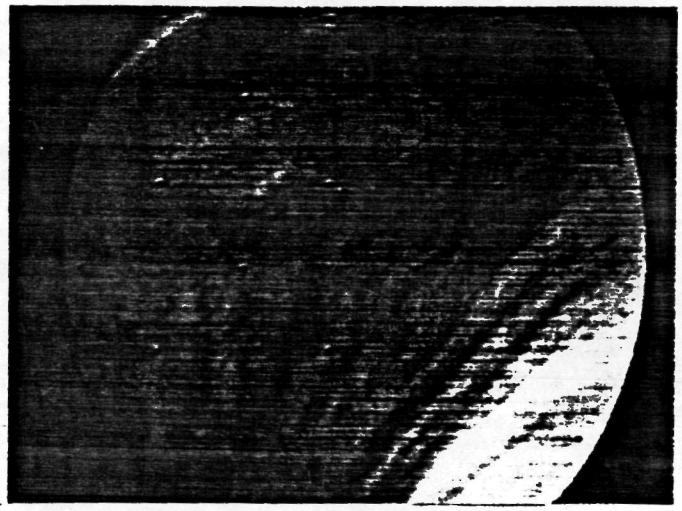

FDS # 65343 09 01 56 GMT

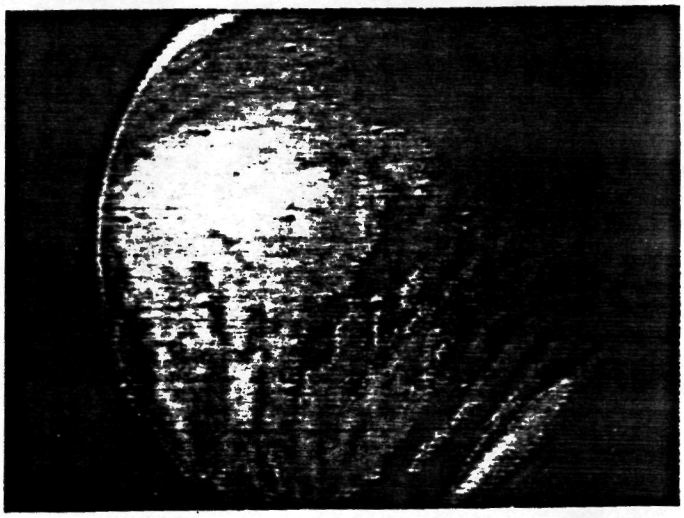

FDS # 65473 10 32 56 GMT

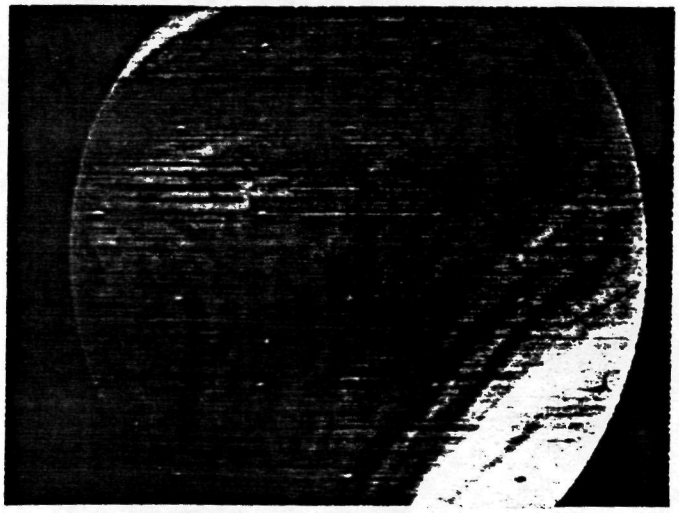

FDS # 65473 10 32 56 GMT

UNCORRECTED VERSION

NORMALIZED VERSION

J. DAY 40, 1974

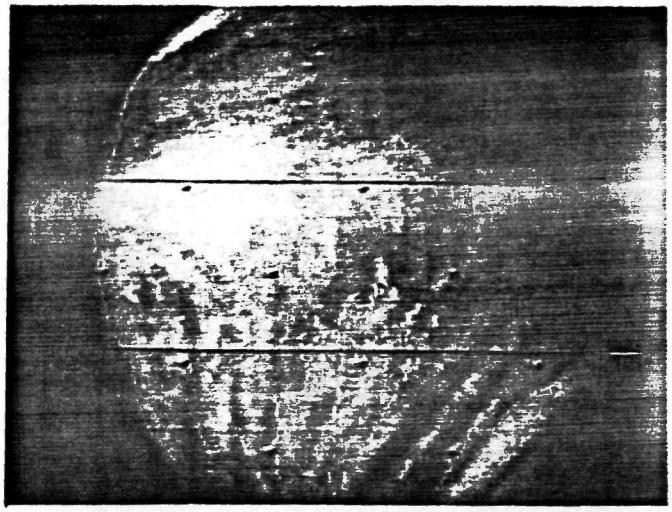

FDS# 65623 12 17 56 GMT

FDS# 65623 12 17 56 GMT

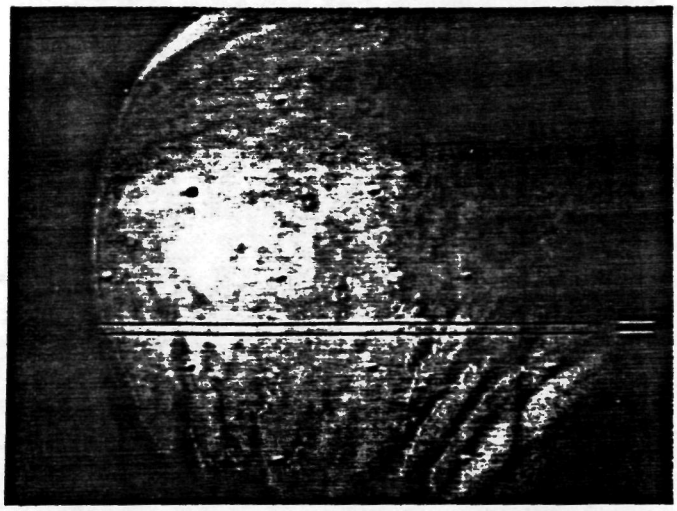

FDS# 65787 14 12 44 GMT

FDS# 65787 14 12 44 GMT

FDS# 65923 15 47 56 GMT

FDS# 65923 15 47 56 GMT

UNCORRECTED VERSION

NORMALIZED VERSION

J. DAY 40,1974

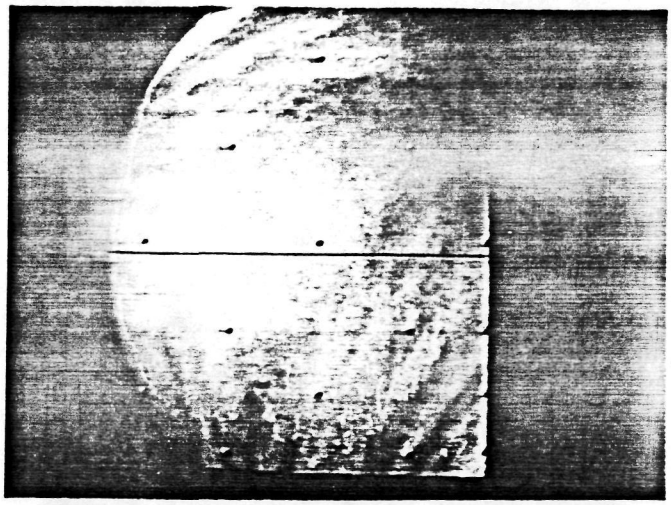

FDS# 66067 17 28 44 GMT

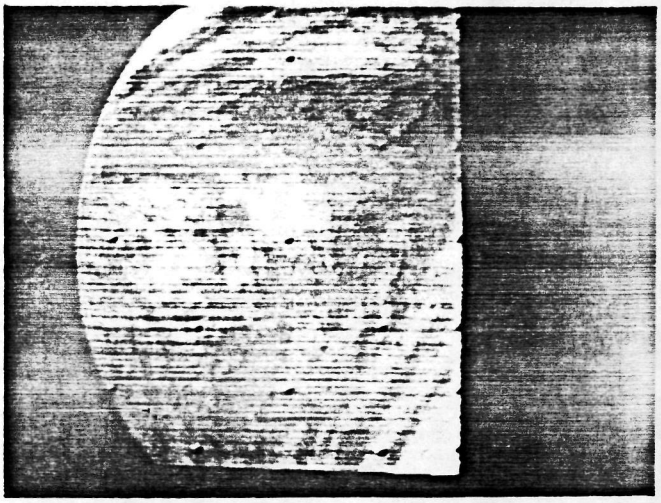

FDS# 66067 17 28 44 GMT

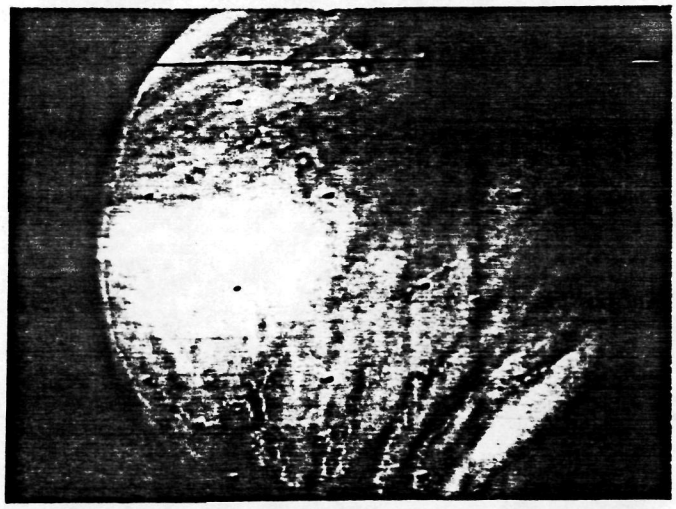

FDS# 66223 19 17 56 GMT

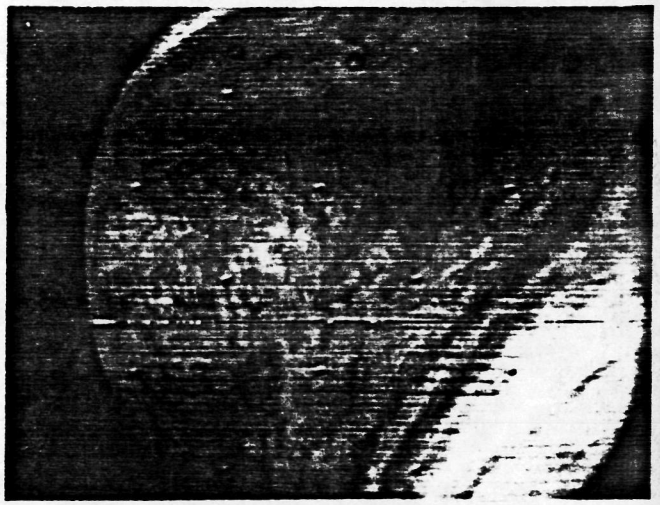

FDS# 66223 19 17 56 GMT

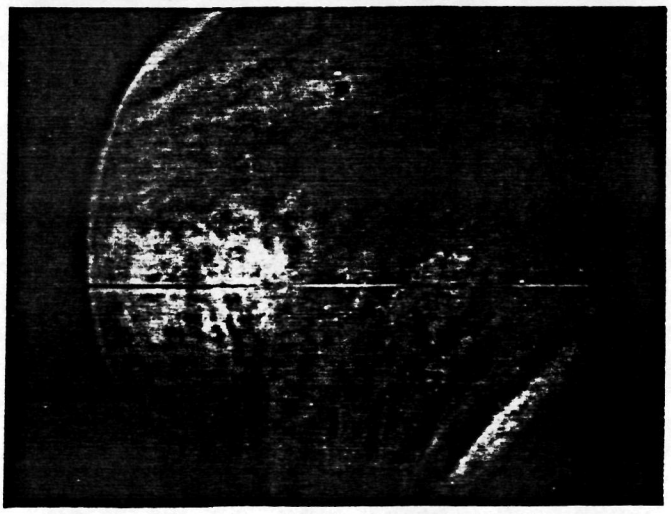

FDS# 66380 21 07 50 GMT

FDS# 66380 21 07 50 GMT

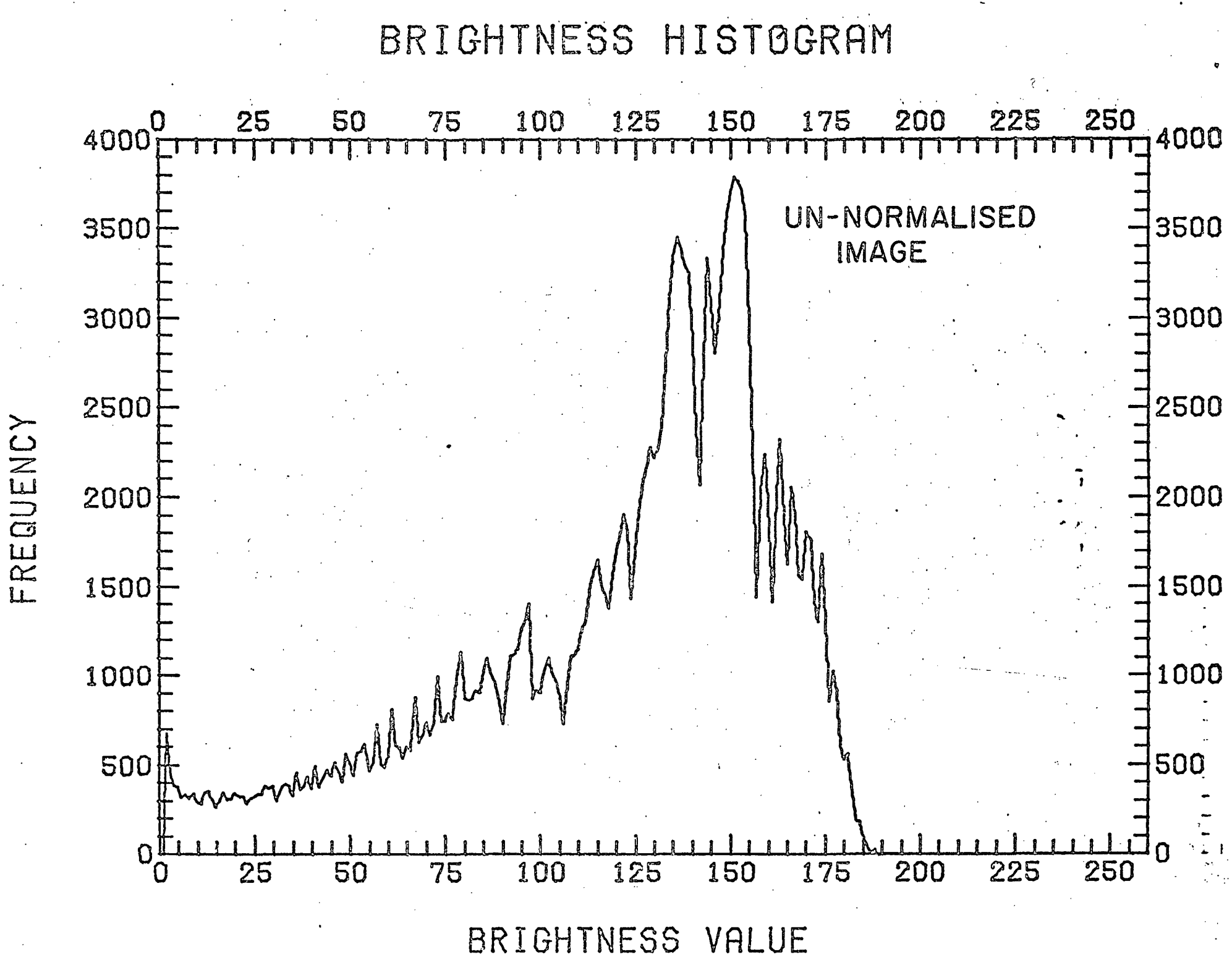
BRIGHTNESS HISTOGRAM
UN-NORMALISED
IMAGE
FREQUENCY
BRIGHTNESS VALUE
0
25
50
75
100
125
150
175
200
225
250
500
1000
1500
2000
2500
3000
3500
4000

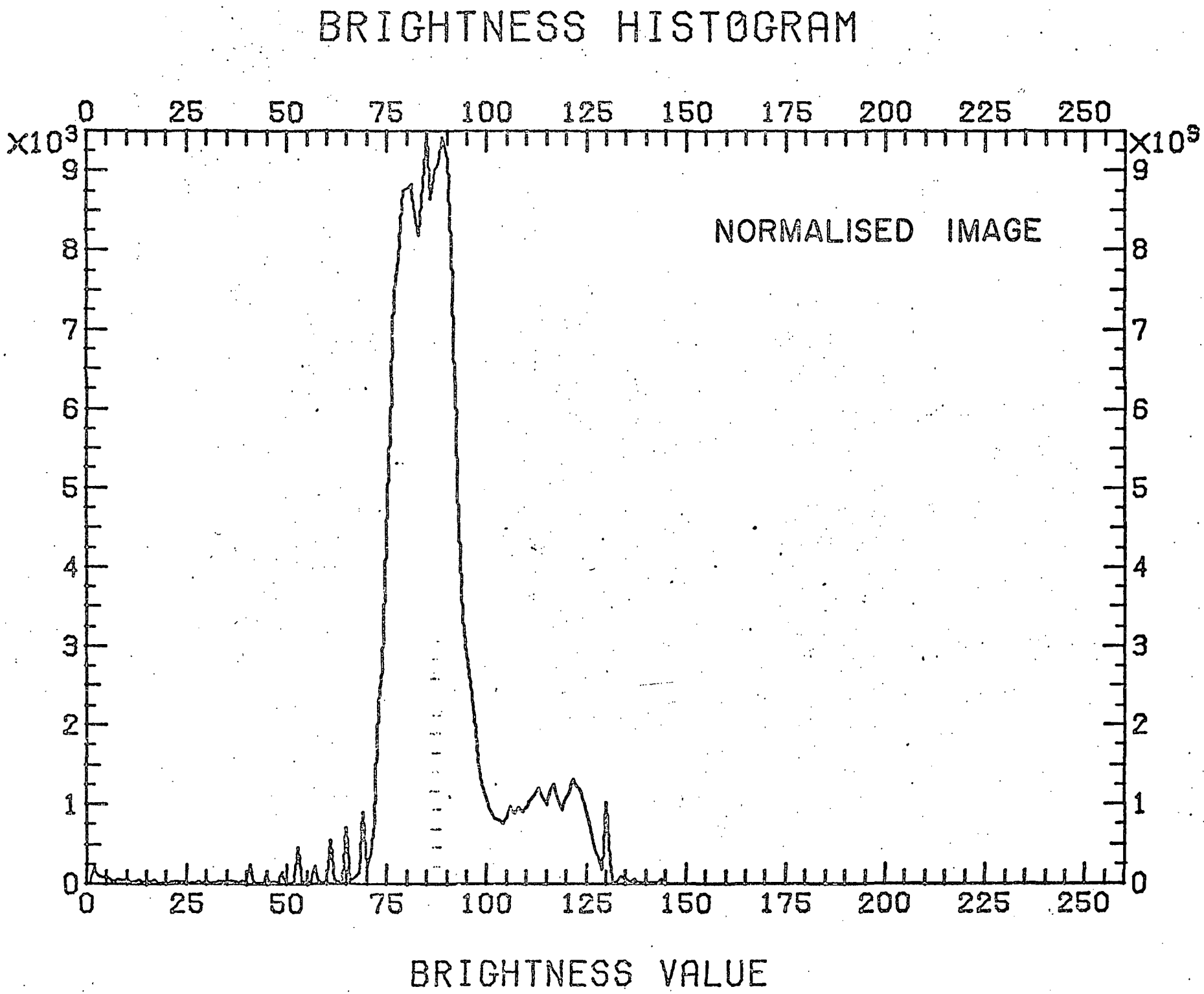
BRIGHTNESS HISTOGRAM
NORMALISED IMAGE
FREQUENCY
X10³
BRIGHTNESS VALUE
0
25
50
75
100
125
150
175
200
225
250
1
2
3
4
5
6
7
8
9

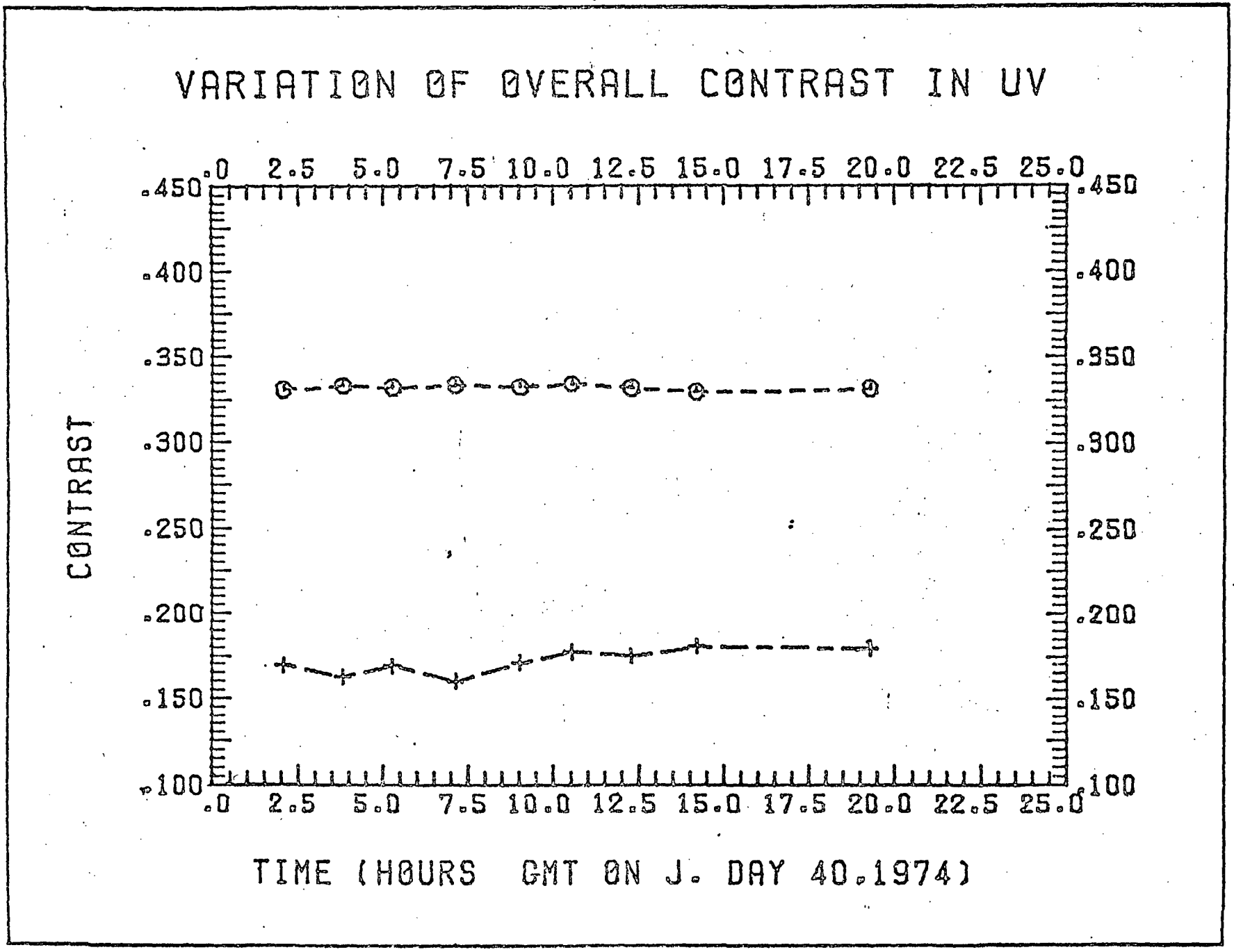
VARIATION OF OVERALL CONTRAST IN UV
CONTRAST
.450
.400
.350
.300
.250
.200
.150
.100
.0 2.5 5.0 7.5 10.0 12.5 15.0 17.5 20.0 22.5 25.0
TIME (HOURS GMT ON J. DAY 40.1974)

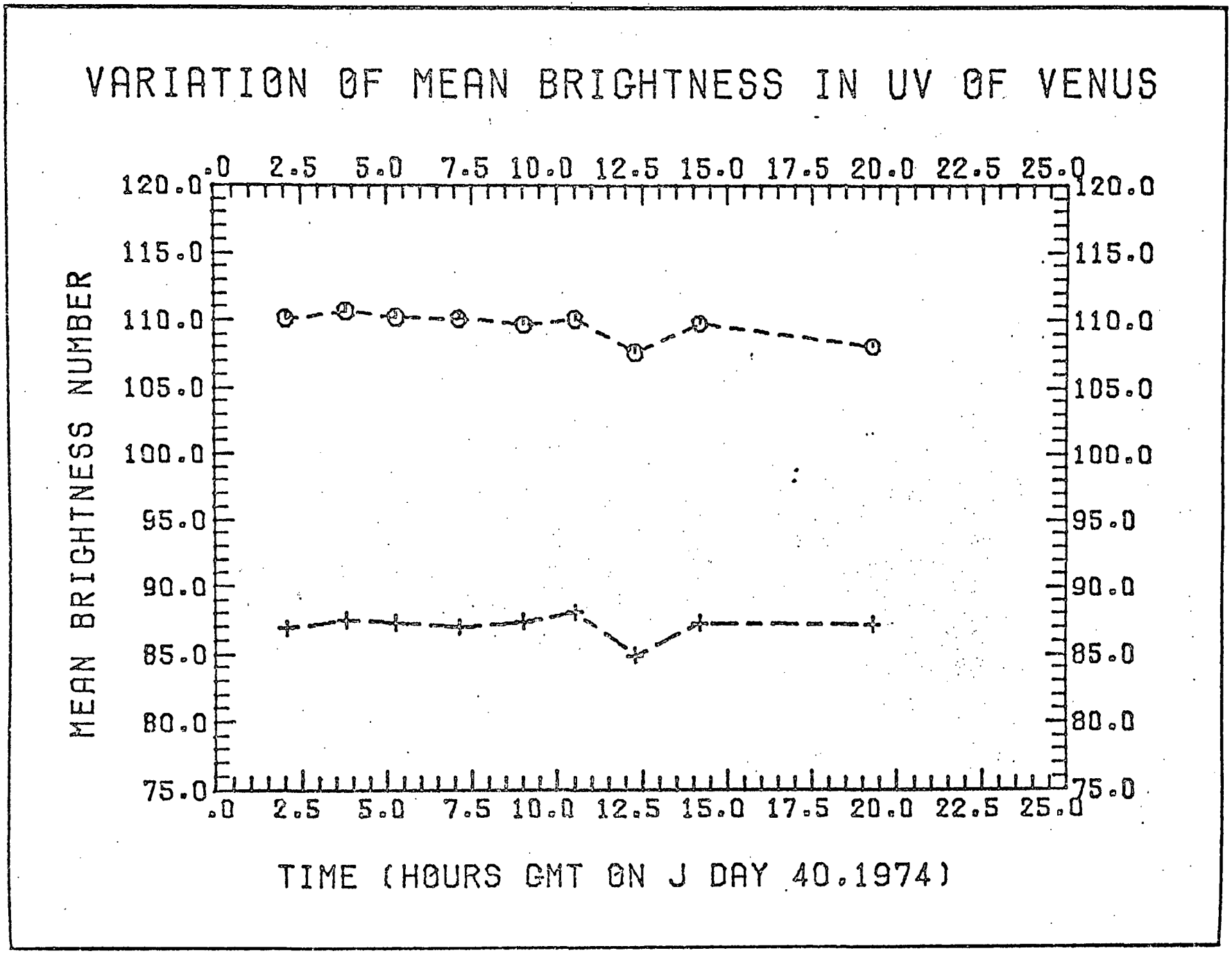
VARIATION OF MEAN BRIGHTNESS IN UV OF VENUS
MEAN BRIGHTNESS NUMBER
120.0
115.0
110.0
105.0
100.0
95.0
90.0
85.0
80.0
75.0
.0
2.5
5.0
7.5
10.0
12.5
15.0
17.5
20.0
22.5
25.0
TIME (HOURS GMT ON J DAY 40.1974)

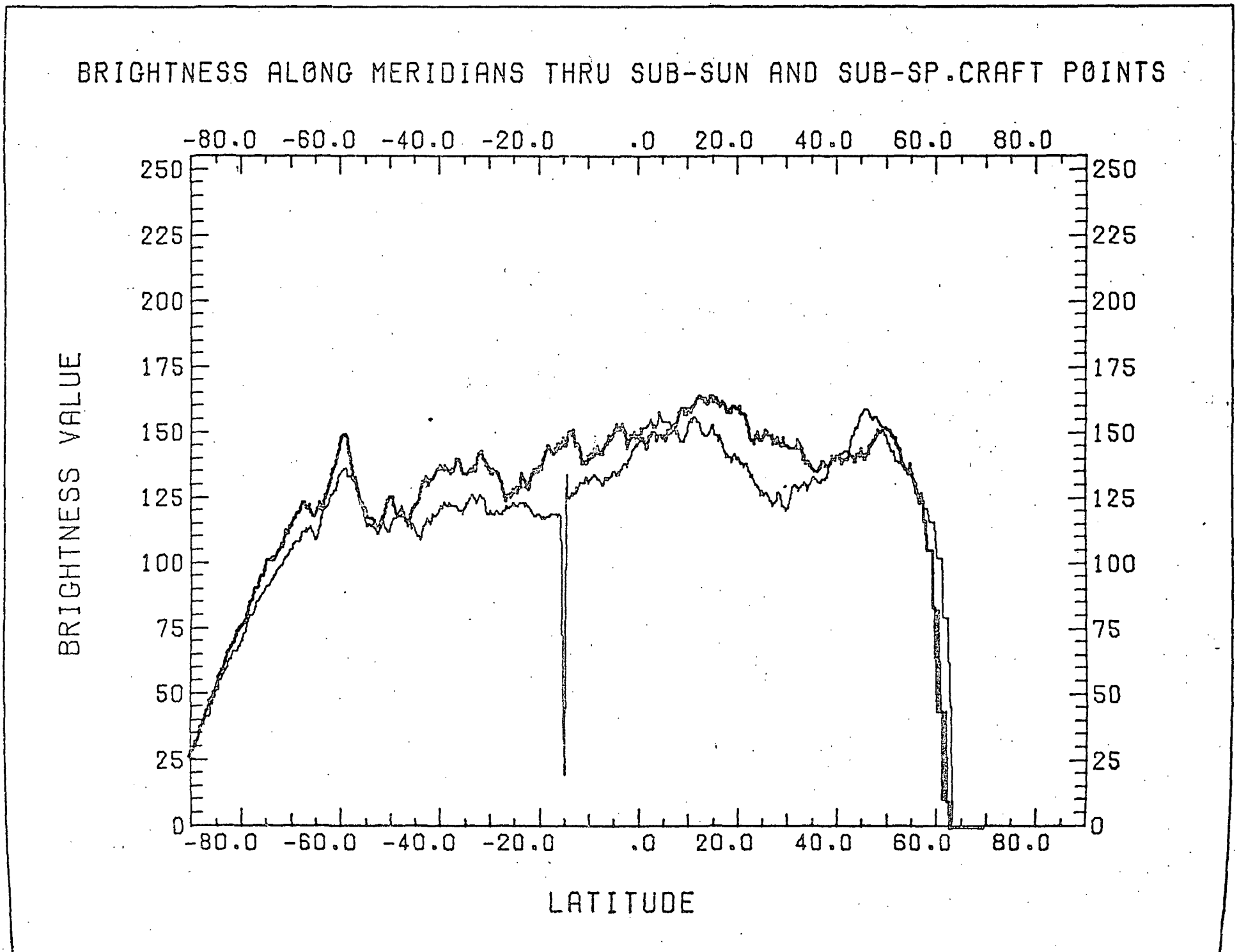
BRIGHTNESS ALONG MERIDIANS THRU SUB-SUN AND SUB-SP.CRAFT POINTS
-80.0 -60.0 -40.0 -20.0 .0 20.0 40.0 60.0 80.0
250
225
200
175
150
125
100
75
50
25
0
BRIGHTNESS VALUE
LATITUDE

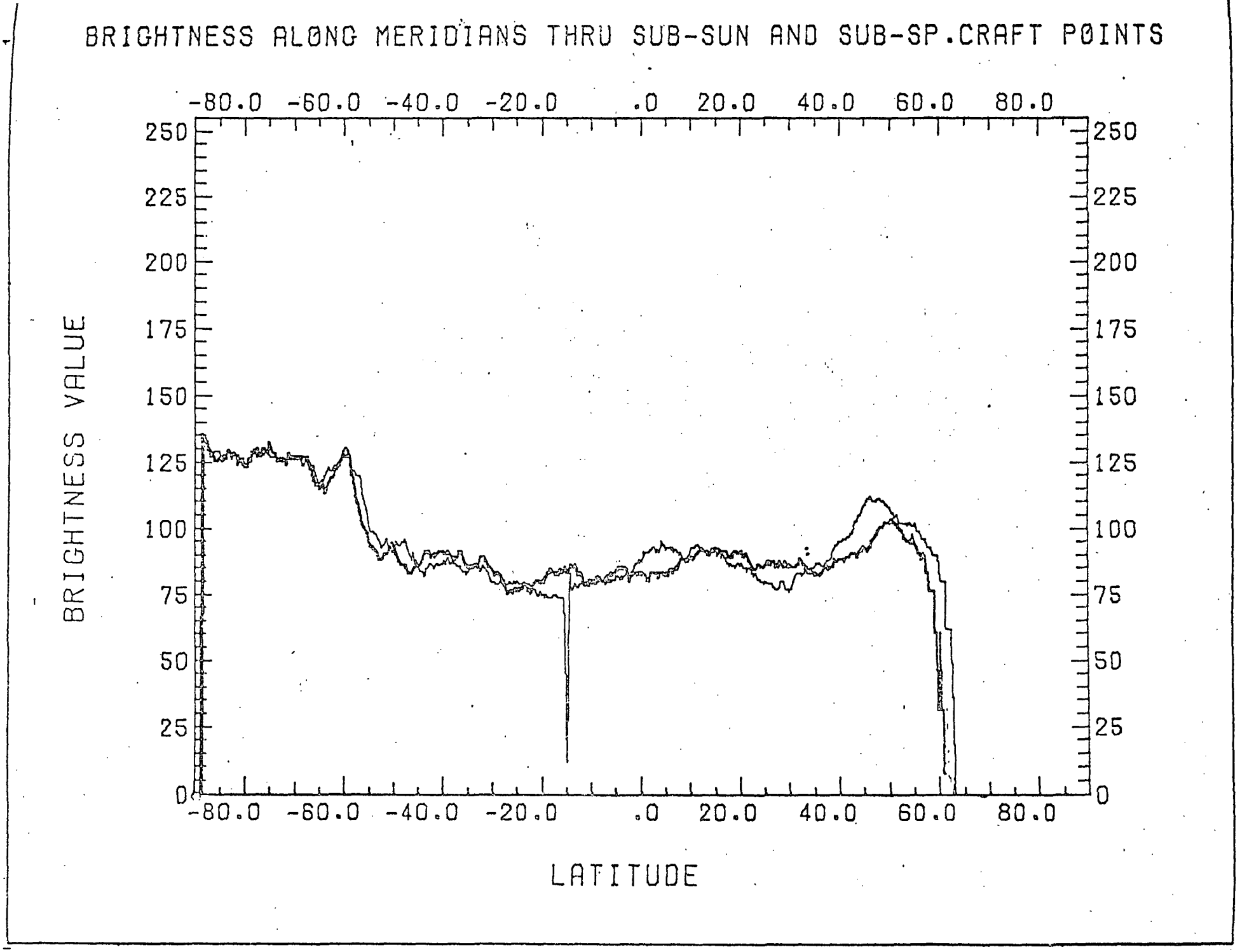
BRIGHTNESS ALONG MERIDIANS THRU SUB-SUN AND SUB-SP.CRAFT POINTS
-80.0 -60.0 -40.0 -20.0 .0 20.0 40.0 60.0 80.0
250
225
200
175
150
125
100
75
50
25
0
BRIGHTNESS VALUE
LATITUDE

APPENDIX B

NAVIGATION OF MARINER 10 IMAGES OF VENUS

by

Dennis Phillips and Sanjay Limaye

Navigation of Mariner 10 Images of Venus

Dennis Phillips and Sanjay Limaye

Abstract

In order to make quantitative use of spacecraft images such as those obtained from Mariner 10 flyby mission to Venus it is necessary to obtain a navigation transform which enables one to determine the planet coordinates of a feature from its image coordinates. The problem of obtaining the required navigation for images of Venus is complicated by the lack of any landmarks, as are available in the cases of the Earth, Moon, Mercury and Mars.

A procedure is described herein to obtain the navigation transform using a least squares solution to the bright limb of the planet and a knowledge of the spacecraft position relative to the planet. The procedure requires that a "sufficient" portion of the bright limb be present in the image and that the attitude of the spacecraft camera be specified.

The quality of the navigation is judged by the consistency among several consecutive frames. The scheme is easily applicable to snapshots of other planets as will be available, for example from the proposed Mariner missions to Saturn, Jupiter and Uranus.

Introduction

In order to determine the absolute position on a planet of a point seen in a spacecraft image of that planet, it is necessary to obtain a navigation transform. The problem is made more difficult for images of Venus as they do not show any "landmarks" which are stationary relative to the planet. The error in the relative position of points is dependent on the accuracy and precision of the navigation transform. The precision of the navigation transform is limited by the spatial resolution of the imaging system and any smear in the images caused by the relative motion of the spacecraft with respect to the planet. A good navigation transform is a pre-requisite for obtaining displacement of mobile features in the images, and accurate velocity measurements additionally necessitate a certain minimal time interval between the image pairs selected for such measurements. Table 1 indicates the tracking error introduced for a given accuracy of the navigation transform for various time intervals.

A navigation transform is obtained by determining the transformation matrix which will transform an image coordinate vector into its counterpart in planet centered polar coordinates. Frequently this is done by selecting and measuring a few landmarkes in image coordinates whose planet coordinates are known (Smith and Phillips, 1972). Due to the lack of landmarks in images of Venus the image coordinate vector has to be defined in terms of other parameters. This procedure is described in the following sections.

Table I

TRACKING ERROR FOR VARIOUS GROUND RESOLUTIONS AND TIME INTERVALS IN M/SEC

TIME	RESOLUTION					
	10 KM	20 KM	30 KM	40 KM	50 KM	60 KM
10 MIN	16.7	33.3	50.0	66.7	83.3	100.0 M/SEC
20	8.3	16.7	25.0	33.3	41.7	50.0
30	5.6	11.1	16.7	22.2	27.8	33.3
40	4.2	8.3	12.5	16.7	20.8	25.0
60	2.8	5.6	8.3	11.1	13.9	16.9
90	1.9	3.7	5.6	7.4	9.3	11.1
120	1.4	2.8	4.2	5.6	7.4	8.3

The Navigation Transform:

The first step necessary to obtaining an image navigation transform is the identification of an image coordinate vector whose planet coordinate counterpart is known. The extensive cloud cover on Venus evolves with time and it is necessary to look for other "natural" points to describe the image coordinate vector. It seems that this is likely to be the case for images of Jupiter and Saturn too. One natural candidate is the sub-spacecraft point which is easily identifiable in whole disc pictures of a spherical object. From a knowledge of the spacecraft orbit the planet coordinates of the sub-spacecraft point on the planet surface is generally known with reasonable accuracy.

A second point is needed in order to determine how the image is rotated around the ray joining the spacecraft to the planet's center. How this point is to be chosen is not immediately clear. However, information about the imaging system, its position relative to the spacecraft and the trajectory of the spacecraft relative to the planet generally contains enough information to compute the image coordinate position of a second reference point. For example, Mariner 10 which is a three axis gyro-stablized spacecraft has two sensors, a Canopus sensor and a sun-sensor to determine the orientation of the spacecraft in its orbit. Thus from the known celestial positions of either of the stars the sub-star reference point on the planet is known and its image coordinates relative to the first reference point namely the sub-spacecraft point can be computed. This requires knowledge of the spacecraft design. Attitudes of spin-scan cameras need be determined in a similar way also.

The necessity to use the sub-spacecraft point as one of the reference points means that its position be known by some means, in the specific image. Perhaps the most reliable way to obtain the image coordinates of the sub-spacecraft point for a spherical object is to use the bright limb as the reference circle and determine its center of curvature. This problem is made slightly easier if the radius of curvature in the planet image is independently known. A successful planet center determination requires that the individual image have a substantial amount of the planet limb. Thus, this navigation scheme can only be used for whole or substantial limb containing images and a modification of this technique need be developed for other images. The navigation problem can be divided into two kinds:

(i) navigation of whole disc or images with a substantial amount of bright limb present, and,

(ii) navigation of images containing little or no limb, e.g. mosaic frames.

Under special circumstances the second class of frames can be navigated by using a modified version of the technique used for the whole disc or "enough limb" images. This technique will be described in a follow-up paper. The whole disc or "enough-limb" frame navigation will now be described in detail.

a. Determination of the sub-spacecraft point

As mentioned earlier this is frequently a case of determining the radius of curvature and the center of curvature for a given arc. In the more general case an ellipse needs to be determined such that it will pass through the points defining the arc. Numerically this involves minimizing the sum:

$$S(x_c,y_c,a,b) = \sum_i \left[\frac{(x_c-x_i)^2}{a^2} + \frac{(y_c-y_i)^2}{b^2} - 1\right]^2$$

In general the line scan direction will be at an angle θ with the axes of the ellipse defining arc, so that the coordinates (x_i,y_i) of the points on the arc and (x_c,y_c) of the center of the ellipse in angular space are defined in terms of:

$$\begin{pmatrix} x \\ y \end{pmatrix} = \begin{pmatrix} \cos\theta & \sin\theta \\ -\sin\theta & \cos\theta \end{pmatrix} \begin{pmatrix} l_i * \text{RDPLIN} \\ e_i * \text{RDPELE} \end{pmatrix}$$

As such there are five unknowns in Equation (1) namely the two numbers giving the ellipse center (x_c,y_c) or equivalently l_c and e_c, the semi-major and semi-minor axes a and b, and the inclination angle θ between the line scan direction and the semi-major axis of the ellipse (the relative camera roll angle). The number of unknowns can be reduced to four if the eccentricity of the ellipse (in other words that of the axisymmetric spheroid) is known a priori such that either of the two axes of the ellipse can be expressed in terms of the other.

The problem is further simplified if the object is known to be spherical. In fact, when the eccentricity, e, of the ellipse is too small to be measured within the resolution of the sampling, including the variables (a,b,e) gives us an over determined problem with associated difficulties. In the case of Venus, from ground-based radar observations, the oblateness has been known to be quite small. Howard, et.al. (1974) report that the fractional differences in the principal moments of inertia of Venus are no larger than 10^{-4}. However in the Mariner 10 images of Venus one does not see the solid surface of the planet but only its cloud cover. Diagnostic studies of the pole-equator thermal contrast at the cloud-top level, Limaye (1975), place an upper limit of a maximum of 14 km in the cloud-top height difference between the equator and the poles for an assumed temperature lapse rate of about 5°K/km at the 80 km altitude. The actual difference in altitude levels of cloud-tops seen in the Mariner 10 images are likely to be smaller, as is the temperature contrast used in arriving at the above figure. Barker and Perry (1975) report that there may be about 3% more carbon dioxide gas above the cloud-tops in the polar latitudes compared to the equatorial latitudes, as indicated by increased absorption in spectroscopic observations. In view of this it may be concluded with reasonable assurance that the cloud-top figure may be considered to be a sphere. The radius of this sphere is as yet left as an unknown.

For the particular case of Venus the expression to be minimized reduces to:

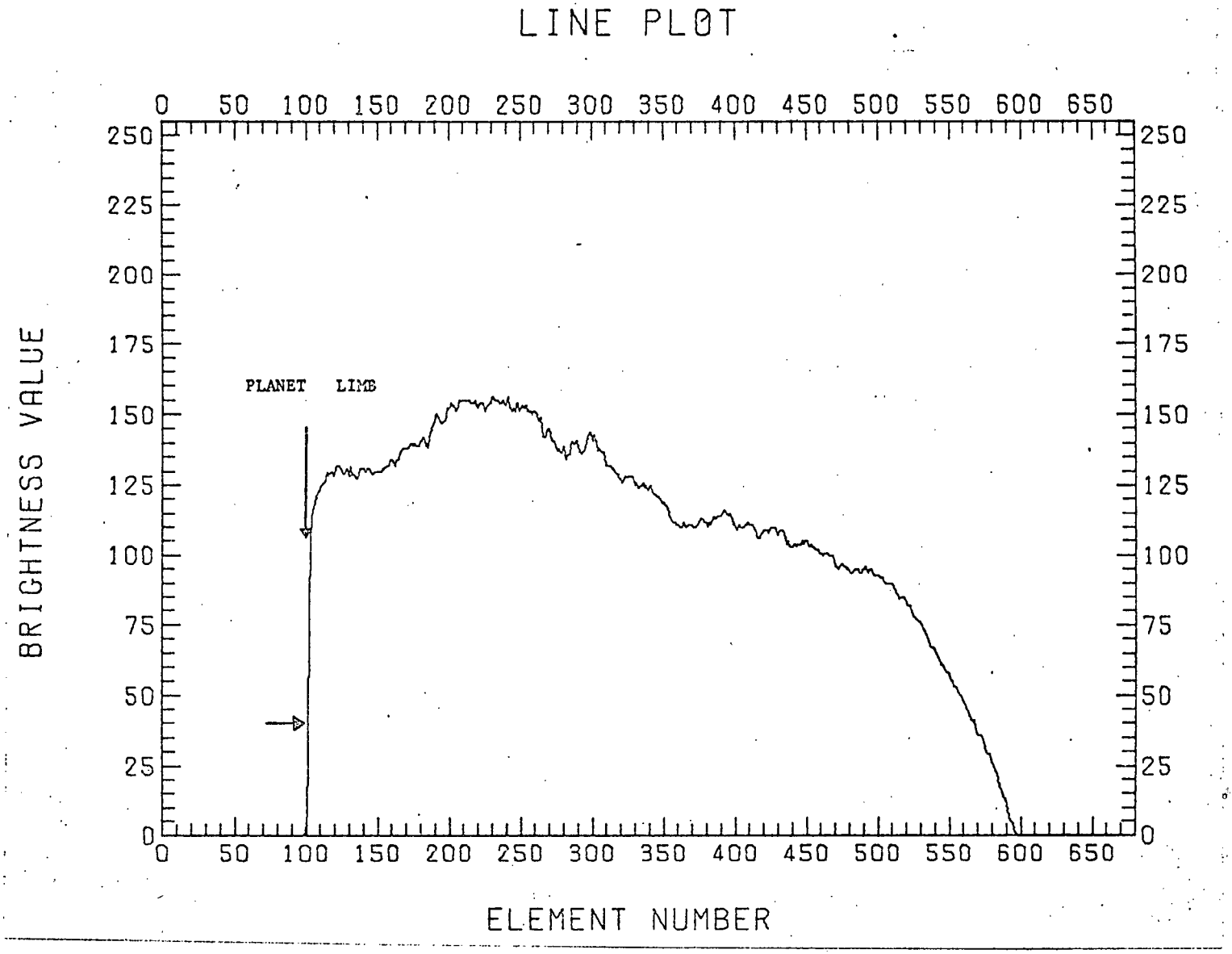

Figure 1. Brightness variation along a scan line. The slope of this curve at any point gives the combined scale height of the gas and scattering aerosol mixture. O'Leary (1975) has determined that the unit slant optical depth generally corresponds to a 40 DN in a FICORed image and occurs at about 6131 km from planet center.

$$S = \sum_i [(x_c-x_i)^2 + (y_c-y_i)^2 - a^2]^2$$

since for a circle a ≡ b and e = 0.
The three unknowns x_c, y_c and a are determined by the constraints:

$$\frac{\partial S}{\partial a} = \sum_i \frac{\partial}{\partial a} [(x_c-x_i)^2 + (y_c-y_i)^2 - a^2]^2 = 0$$

if a is not independently known.

$$\frac{\partial S}{\partial x_c} = \sum_i \frac{\partial}{\partial x_c} [(x_c-x_i)^2 + (y_c-y_i)^2 - a^2]^2 = 0$$

and,

$$\frac{\partial S}{\partial y_c} = \sum_i \frac{\partial}{\partial y_c} [(x_c-x_i)^2 + (y_c-y_i)^2 - a^2]^2 = 0.$$

In practice the solution is obtained by iteration using the Newton-Raphson scheme.

b. Limb Determination and the Radius of the Cloud-top Figure of Venus

For a planet with a thick atmosphere such as Venus the scans across the limb show a gradual rather than a sharp increase in brightness due to atmospheric scattering (see Figure 1). The points defining the limb in the image have to be chosen with care since they determine the location of the sub-spacecraft point from high resolution limb scans from Mariner 10. O'Leary (1975) has determined that the slant optical depth of unity occurs in the atmosphere of Venus at the 4 mb level or at about 6131 km from the planet center. We have adopted this result to determine the limb location and the radius at the cloud-top level for navigational purposes. The slant optical depth is determined by the relation:

$$I_{\tau_{s=1}} / I_{\tau_{s=\infty}} = (1-e^{-1}) = 0.63.$$

The corresponding level for the limb scan of Figure 1 is indicated therein. Experience with Mariner 10 UV images has shown that frequently the $\tau_{s=1}$ position or the limb position in a given line scan ocurrs at the pixel with digital brightness number closest to 40 for a typical exposure (~78.3 milliseconds). A one resolution element error in a single limb location is not a serious error as it causes a smaller error in the sub-spacecraft point if more than four limb points are used.

c. The Reference Vector

The Mariner 10 cameras were mounted on a scan platform which had only two degrees of freedom - the clock and cone directions. Its orientation relative to the sun-sensor and Canopus sensors was thus fixed if small errors such as scan platform backlash are ignored. A direct consequence of this is that all the scan lines point towards the sun within the combined 3 axis attitude error limits ($\leq \pm 0.4$ degree). Thus, both the sub-solar and the sub-spacecraft points are, within the attitude error limits, on the same scan line. It is obvious that the extent of parallelism of the vidicon scan lines with the line passing through the sub-solar and sub-spacecraft points is governed by the ratio of the separation of the two points to the small roll error.

Once the scan line number of the sub-solar point is known, its sample element number is easily determined knowing the angular separation of the sub-solar point relative to the sub-spacecraft point and the average angular size of a sample element in the scan direction.

Thus the two reference points defining the reference vector are now known, both in the image coordinates and the planet coordinates and the transformation matrix can be determined as two successive rotation operations - the first one brings the sub-spacecraft point to coincide with its image coordinate and the next one brings the sun onto the same scan line.

The Transforms:

a. The transformation T such that:

$(l,e) = T(\lambda,\phi)$

$(\lambda,\phi) = T^{-1}(l,e)$ is required.

Let us first state the properties of a Euclidean transformation in a finite dimensional Cartesian coordinate system. A Euclidean transformation preserves both the distances between points and angles between intersecting rays. All Euclidean transformations can be characterized as

$$X_v = RX_s + b$$

where R is a rotational matrix and b is a displacement vector. Let us assign the subscript s to vectors in our satellite centered coordinate system and the subscript v to vectors in our Venus centered coordinate system.

II. Coordinate Systems

Let our spacecraft-centered coordinate system (Figure 2) be defined as follows:

The x axis points from the focal point of the image camera through the center point of the vidicon frame. Our y axis originates at the same point, is perpendicular to the x axis and is parallel to the scan lines going from

Figure 2. The Venus centered coordinate system.

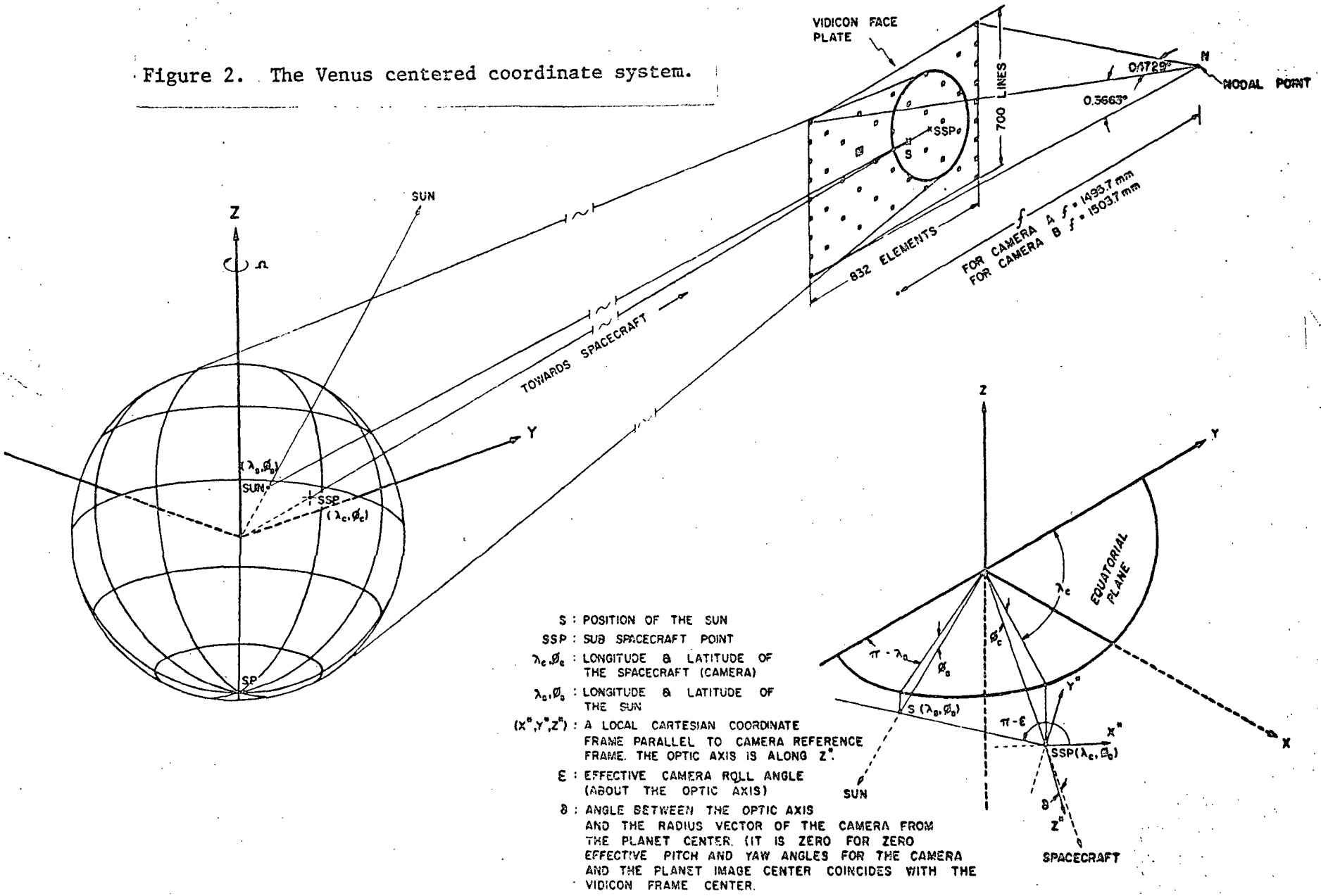

S : POSITION OF THE SUN

SSP : SUB SPACECRAFT POINT

λ_c, ϕ_c : LONGITUDE & LATITUDE OF THE SPACECRAFT (CAMERA)

λ_0, ϕ_0 : LONGITUDE & LATITUDE OF THE SUN

(X^*, Y^*, Z^*) : A LOCAL CARTESIAN COORDINATE FRAME PARALLEL TO CAMERA REFERENCE FRAME. THE OPTIC AXIS IS ALONG Z^*.

ε : EFFECTIVE CAMERA ROLL ANGLE (ABOUT THE OPTIC AXIS)

δ : ANGLE BETWEEN THE OPTIC AXIS AND THE RADIUS VECTOR OF THE CAMERA FROM THE PLANET CENTER. (IT IS ZERO FOR ZERO EFFECTIVE PITCH AND YAW ANGLES FOR THE CAMERA AND THE PLANET IMAGE CENTER COINCIDES WITH THE VIDICON FRAME CENTER.

the right to left direction. The z axis completes a right handed orthogonal coordinate system.

Our Venus centered coordinate system (Figure 2) has its z axis coinciding with the spin axis of Venus and its x axis pointing towards (0°, 0°) of a latitude and longitude coordinate system tied to the planet's surface. The y axis makes the coordinate system right handed.

III. Parameter Base for Transformations

Let us start with the following parameters:

(e_c, l_c) - the displacement of picture coordinates of the center of the planet Venus from the nominal picture center.

(λ_c, ϕ_t) - (Figure 2) the longitude and latitude of the spacecraft's sub-satellite point.

(λ_s, ϕ_s) - (Figure 2) the longitude and latitude of the subsolar point.

h - the altitude of the satellite.

a - Venus radius

From this set of parameters we will derive the rotational matrix R and the displacement vector T.

IV. Derivation of R and b

Let us consider the equation again $X_v = RX_s + b$, where it is understood that "b" and any subscripted "X" are vectors. When we are at the center of the satellite frame $X_s = 0$ and $X_v = b$. Hence b is the vector from the center of Venus to the satellite.

Hence

$$(b) = \begin{pmatrix} (a+h)\cos\phi_c \cos\lambda_c \\ (a+h)\cos\phi_c \sin\lambda_c \\ (a+h)\sin\phi_c \end{pmatrix}.$$

Now we can restrict our attention to finding the rotational matrix R. Consider the action of R on the vector X_v^s pointing towards the subsatellite points

$$X_s^s = \begin{pmatrix} \cos(l_c * \text{RDPLIN}) * \cos(e_c * \text{RDPELE}) \\ \cos(l_c * \text{RDPLIN}) * \sin(e_c * \text{RDPELE}) \\ \sin(l_c * \text{RDPLIN}) \end{pmatrix}$$

Now $X_v = hRX_s^s + b$,

and $X_v = ba/(a+h)$,

hence, $RX_s^s = X_v - b = -b/(a+h)$.

If we determine how R rotates one more linearly independent vector, we can determine R.

Consider the vector from the center of Venus to the subsolar point:

$$X_v^{ss} = \begin{pmatrix} a\cos\phi_s^s \cos\lambda_s^s \\ a\cos\phi_s^s \sin\lambda_s^s \\ a\sin\phi_s^s \end{pmatrix} .$$

Let us find the angle γ between the vector from the spacecraft to the center of Venus and the vector from the spacecraft to the subsolar point.

$$\gamma = -[\arccos b \cdot (X_v^{ss}-b)/(||b||*||X_v^{ss}-b||)].$$

Let us now find the vector X_s^{ss} pointing from the spacecraft to the subsolar point in the satellite coordinate system.

$$X_s^{ss} = (||X_s^{ss}-b||)*\begin{pmatrix} \cos(1_c^c*RDPLIN)*\cos(e_c^c*RDPELE+\gamma) \\ \cos(1_c^c*RDPLIN)*\sin(e_c^c*RDPELE+\gamma) \\ \sin(1_c^c*RDPLIN). \end{pmatrix}$$

Hence, $X_v^{ss} = RX_s^{ss} + b$

and $RX_s^{ss} = b-X_v^{ss}$.

Finally $RX_s^{ss}/||X_s^{ss}|| = (b-X_v^{ss})/||b-X_v^{ss}||$.

This gives us our second linearly independent vector and, hence, R is determined.

V. Derivation of T and T^{-1}

Let us now discuss how R and b can be used to find the transformations T and T^{-1}.

A. Finding T or the transformation from Venus coordinates to Picture Image Coordinates:

Let us start with a longitude-latitude pair (λ,ϕ) of Venus coordinates.

Then

$$X_v = \begin{pmatrix} a\ \cos\lambda\cos\phi \\ a\ \sin\lambda\cos\phi \\ a\ \sin\phi \end{pmatrix} .$$

Aside from the mislocation of the sub-spacecraft point the navigational errors arise mainly due to:

(i) roll, pitch, and yaw error

(ii) remaining geometric distortions in the vidicon image.

Of these, the corrections for roll pitch and yaw errors can be estimated from camera pointing information. The errors introduced by geometric distortions are difficult if not impossible to obtain without measuring location of nearby reseaus and determining local image geometry. However, these errors are generally (in GEOMED images only) comparable to the resolution of the vidicon and can be ignored.

Summary

A technique has been described herein to navigate planetary images obtained from spacecraft with vidicon type cameras. At present this has been used for Mariner 10 images of Venus having a substantial portion of the bright limb. Use of pattern recognition techniques and some idea of the atmospheric (cloud) motions will allow this technique to be used for higher ground resolution mosaic images also. Work is now in progress along these lines.

Acknowledgements:

The authors thank Messrs. Robert Krauss and Eric Smith of the University of Wisconsin Space Science and Engineering Center for their help in the implementation of the navigation scheme on McIDAS, and Mr. K. Klaasen and Mr. G. E. Danielson of the Jet Propulsion Laboratory for their assistance with the SEDR output.

This research was supported by JPL Contract 953034 and by NASA Grant No. NGR-50-002-189.

REFERENCES

Barker, E.S. and M.A. Perry, 1975: Semi Periodic Variations in CO_2 Abundance on Venus, ICARUS, (25), 282-295.

Howard, H.T., G.L. Tyler, G. Fjeldbo, A.J. Kliore, G.S. Levy, D.L. Brunn, R. Dickinson, R.E. Edelson, W.L. Martin, R.B. Postal, B. Seidel, T.T. Sesplauleis, Z.Z. Zygielbaum, P.B. Esposito, J.D. Anderson, I.I. Shapiro, and R.D. Rosenberg, 1974: Venus: Mass, Gravity Field, Atmosphere, and Ionosphere as Measured by the Mariner 10 Dual Frequency Radio System. Science, (183), 1297-1306.

Limaye S.S. 1975: Pole-Equator Temperature Contrast on Venus and its Implications. Space Science and Engineering Center, University of Wisconsin, Madison, Report to NASA.

O'Leary, B., 1975: Venus: Vertical Structure of Stratospheric Hazes from Mariner 10 Pictures, Journ. Atmos. Sci. (32), 1091-1100.

Smith, E.A., and D.R. Phillips, 1972: Automated Cloud Tracking Using Precisely Aligned Digital ATS Pictures. IEEE Trans. on Computers, (C-21), 715-729.